The Astronomical Journal, 129:2869–2886, 2005 June

THE STATISTICAL ASTEROID MODEL. I. THE MAIN-BELT POPULATION FOR DIAMETERS GREATER THAN 1 KILOMETER

Edward F. Tedesco
Space Science Center, University of New Hampshire, Durham, NH 03824; ed.tedesco@unh.edu

and

Alberto Cellino and Vincenzo Zappalá
INAF - Osservatorio Astronomico di Torino, 10025 Pino Torinese, Torino, Italy; cellino@to.astro.it, zappala@to.astro.it
Received 2002 July 10; accepted 2005 January 31

ABSTRACT

We describe the creation of a model of the main asteroid belt whose purpose is to describe the main-belt asteroid size frequency distribution and simulate the number of main-belt asteroids and their fluxes at visual through mid-infrared ($\sim$0.3–70 μm) wavelengths in any area of sky for an arbitrary date. This model is based on a population of $\sim 1.9 \times 10^6$ asteroids obtained from the complete known asteroid sample, plus extrapolation of the size-frequency distributions of 15 asteroid dynamical families and three background populations, to a diameter limit of 1 km. The model is compared with data and other models, example applications are given, planned refinements and extensions to the model are presented, and some implications of the resulting size frequency distribution are discussed.

Key words: infrared: solar system — minor planets, asteroids — solar system: general

1. INTRODUCTION

It is now over 200 years since the discovery of the first asteroid. Yet it is only recently that the question, how many main-belt asteroids are there with diameters greater than N? can be answered, with an uncertainty better than about a factor of 3, for values of N greater than 1 km. The answer to this question is of more than academic interest, for as numerous studies have demonstrated, the asteroid size distribution is important because it provides constraints on models of the original size distribution of the planetesimals formed in the inner solar system and their subsequent evolution (see, e.g., Davis et al. 1989, 2002). It is also a key datum in modeling the numerical size of the population of near-Earth asteroids, accounting for their evolution from the main belt into Earth-orbit-crossing orbits (Michel 1999; Morbidelli et al. 2002), and for providing fundamental data for addressing the asteroid-meteorite connection, zodiacal dust models, and studies of asteroid collisional evolution (e.g., such recent studies as those by Durda & Dermott 1997, Reach 1997, and Durda et al. 1998, hereafter DGJ98), including impact probabilities in the main belt (Dell'Oro et al. 2001).

The limitation of all studies dependent on knowledge of the asteroid size-frequency distribution (SFD) is that, except for the largest (i.e., diameters greater than between about 7 and 20 km, depending on the heliocentric distance, to which size the population is essentially complete), the main-belt asteroid (MBA) SFD is poorly known. For example, recent estimates of the number of MBAs with diameters larger than 1 km range from $\sim 3 \times 10^5$ (Evans et al. 1998) to $\sim 2 \times 10^6$ (this paper).

During 1998 a preliminary version of the Supplemental *IRAS* Minor Planet Survey's (SIMPS; Tedesco et al. 2002) results for asteroids numbered through 8603 was used to update the asteroid database portion of the US Air Force's Celestial Background Scene Descriptor (CBSD;[1] Kennealy et al. 1993). The following year a preliminary version of the model presented here was submitted to the US Air Force for inclusion in the CBSD (Tedesco 2000). The present work is an extension of that described therein.

The model presented in this paper has had a long gestation. Consequently, some of its assumptions, mainly regarding the treatment of asteroid families, are based on evidence that was, until recently, commonly accepted. How our understanding of asteroid families has been changing during this time, mainly as a consequence of the recognition of the importance of the Yarkovsky effect, is extensively discussed by Cellino et al. (2004). Nevertheless, as we demonstrate below, even taking into account that a future development of our statistical model will certainly include a more refined treatment of the consequences of the Yarkovsky effect, the current version is adequate for its purposes and remains a useful tool for those purposes.

Our ultimate goal is to create reliable SFD models for the entire main asteroid belt down to $\sim$100 m and so provide accurate descriptions of the present near-Earth asteroid (NEA) and MBA populations. Extending the SFD to this limit will allow refinement of MBA and NEA origin and evolution models, on which one of the few observable constraints is to start from, or reproduce, the present populations. Such data will also further our understanding of asteroid collisional evolution and the efficiency of the Yarkovsky effect on the dynamical lifetimes of small asteroids.

Results from the model presented here have been used by Hildebrand et al. (2001a, 2001b), Ivezić et al. (2001), Davis et al. (2002), Tedesco & Désert (2002), and Morbidelli et al. (2002) and were used in planning *Spitzer Space Telescope* (formerly *SIRTF*) asteroid observations (e.g., Hanner & Cruikshank 2000). Thus, although work on a more refined model is well under way, making use of a tenfold larger known asteroid population and advances in understanding the mechanisms of family formation and evolution, we are publishing this version of the model to document the results referred to in the studies mentioned here.

[1] Various US Defense Department branches use the outputs of the CBSD models (tables and images) in sensor simulations. The point-source component of the CBSD model simulates the contribution from the celestial background, including asteroids, in the wavelength regime 0.3–30 μm with a positional accuracy of 2″.

2. SIZE-FREQUENCY DISTRIBUTION MODELS

Because measured diameters are available for fewer than 5% of the known asteroids, past studies that published SFDs have actually modeled the absolute magnitude distribution and then, using a variety of approximations, converted that to a "size"-frequency distribution (e.g., Farinella & Davis 1994; DGJ98). A general limitation of these analyses has been a number of rather crude assumptions concerning the distribution of asteroid albedos.

Here we have first estimated the diameters of MBAs numbered through 8603, based on an analysis of the albedo distribution among objects belonging to asteroid families and different regions of the main belt and applying suitable bias corrections when required (see § 2.1). After this we work in diameter-frequency space. This approach more directly produces a reliable *size*-frequency distribution because we can make a fairly good statistical estimate of the diameters for those asteroids lacking any physical measurements from which a diameter could otherwise be estimated.

We define MBAs as those with orbits between the 4:1 and 2:1 mean-motion resonances with Jupiter, i.e., those with orbital semimajor axes between 2.064 and 3.278 AU and with modest inclinations ($<25^\circ$) and eccentricities (<0.3). On the plane of the sky the vast majority of MBAs are found at ecliptic latitudes between $\sim\pm 20^\circ$.

The results presented here are based on an analysis starting in 1998 April, when the known population was 38,629 (of which 8603 were numbered). With the exception of Figure 1, for which it does not matter, the analysis presented herein is based on this set of 8603 numbered asteroids. The orbital data used in this study were obtained from the Lowell Observatory and the Minor Planet Center (MPC) ftp sites.[2]

It has long been recognized that the SFD for at least some asteroid families differs from that for nonfamily asteroids. Available observational evidence indicates that families are characterized by much steeper slopes of the SFD with respect to nonfamily ("background") asteroids in the interval of sizes for which family memberships are supposed to be essentially complete (Cellino et al. 1991; Zappalà & Cellino 1996; Tanga et al. 1999). Moreover, different SFD slopes have been determined for different families (Tanga et al. 1999). Thus, for diameters below the completeness size the MBA SFD to diameters of about 1 km can be estimated from reasonable extrapolations of different SFDs of family and background populations. However, this general assumption is questionable, according to recent results based on the Sloan Digital Sky Survey (SDSS). In particular, Morbidelli et al. (2003) conclude that at small sizes the SFDs of many families can actually be shallower than those exhibited by nearby background asteroids. On the other hand, as discussed by Cellino et al. (2004), this issue is still open in several respects. Therefore, in this paper we use the assumption that family SFDs are steeper than the background SFD, and thus, that it is reasonable to treat them as we have.

Accordingly, the statistical asteroid model (SAM) makes a distinction between family and nonfamily asteroids. The current version of SAM is designed to simulate the population of objects larger than 1 km located in the main asteroid belt. That is, Hungarias, NEAs, Cybeles, Hildas, Trojans, Centaurs, and trans-Neptunian objects are not included. Rather than using a single SFD or several SFDs—one for each of several "regions" in the main belt (e.g., as done by Kuiper et al. [1958] in the McDonald Survey, Van Houten et al. [1970] in the Palomar Leiden Survey [PLS], and Jedicke & Metcalfe [1998, hereafter JM98] in analyzing Spacewatch Survey data)—SAM divides the main belt into 15 "family" and three "background" populations and estimates an SFD for each. The completed model consists of two "modules": one for the known asteroids and a second for the statistical asteroids generated as described below.

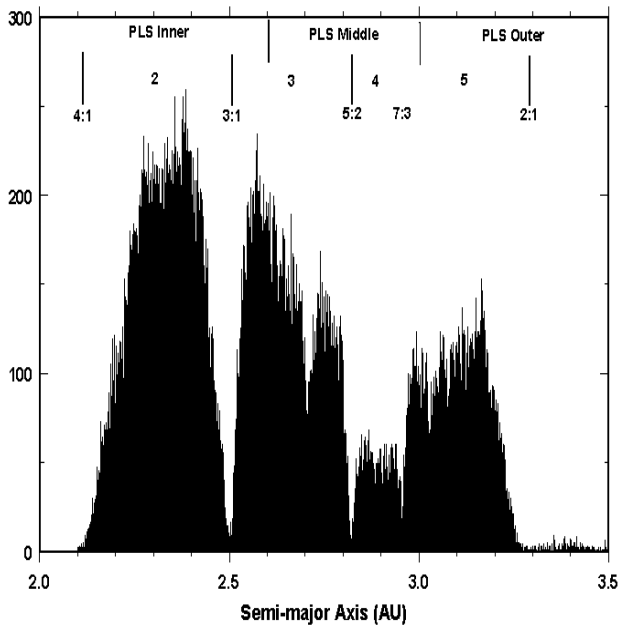

FIG. 1.—MBA semimajor axis histogram for 58,282 asteroids with known orbits as of 1999 December. The histogram bin width is 0.001 AU.

Figure 1 is an uncorrected semimajor axis (a) histogram for MBAs. Shown are the three arbitrary regions into which the earlier studies noted above divided the main belt: inner (2.0 AU $\leq a <$ 2.6 AU), middle (2.6 AU $\leq a <$ 3.0 AU), and outer (3.0 AU $\leq a \leq$ 3.5 AU). Also shown are the four equally arbitrary "zones" (2–5 in this region), defined by major Kirkwood gaps and used by Tedesco (1979)[3] to derive bias completeness factors from which the true distribution of asteroids with diameters greater than about 10 km was estimated. Gradie & Tedesco (1982) used these bias factors in estimating the distribution of the taxonomic classes with heliocentric distance, and a version of this distribution (from Gradie et al. 1989), in turn, together with mean albedos for the major taxonomic classes, was used by JM98) in converting their absolute magnitudes to sizes. JM98, however, chose not to create an SFD, per se.

The *observed* MBA SFD is that created using only the complete known population, i.e., those MBAs with mean apparent opposition V magnitudes, $V(a, 0) < 15.75$.[4] This is the $V(a, 0)$ to which the asteroid inventory is believed to be essentially complete, i.e., virtually all asteroids brighter than this have been discovered (Zappalà & Cellino 1996; JM98). This corresponds

[2] Available at ftp://ftp.lowell.edu/pub/elgb/astorb.html and ftp://cfa-ftp.harvard.edu/pub/MPCORB, respectively.

[3] Tedesco used proper semimajor axes, while the other studies noted here, including the present one, use osculating semimajor axes. The difference between proper and osculating semimajor axes is generally less than a few times 0.001 AU except close to resonances where the uncertainty in the proper semimajor axes exceeds this value, if they can be calculated at all.

[4] The expression $V(a, 0) = H + 5 \log [a(a - 1)]$, where H is the absolute magnitude in the system defined by Bowell et al. (1989), adopted by IAU Commission 20 during the 1990 IAU General Assembly, and the first listing using this system published later that year (Tedesco 1990). We include $V(a, 0)$ down to 15.74 because the 15.5 $V(a, 0)$ magnitude bin used in the bias-correction procedure extends from 15.25 to 15.74, inclusive.

TABLE 1
DEFINITION OF ALBEDO (p_H) CLASSES

Albedo Class	$p_H >$	$p_H \leq$	Log Mean p_H
Low	0.020	0.089	0.05
Intermediate	0.089	0.112	0.10
Moderate	0.112	0.355	0.20
High	0.355	0.526	0.45

to a total of no more than 4500 MBAs[5] (see § 4.3 for further discussion of this point) and, for a location near the middle of the main belt ($a \sim 2.7$ AU), to diameters between about 7 km (for albedo 0.45) and 20 km (for albedo 0.05). Models must be used to estimate the number of asteroids smaller than this.

The SFD varies with location in the asteroid belt and is locally determined by the combination of different groups of objects, some of which are members of dynamical asteroid families and some of which are not, each with their own SFD, some possibly exhibiting structure as discussed in § 4.3. As noted above, we model the main asteroid belt below the completeness limit using 18 different SFDs: one for each of the 15 major Hirayama dynamical families, as defined by Zappalà et al. (1995), plus three for the "background" population. Section 2.1 describes the creation of the background population model and § 2.2 that of the family population models.

2.1. *The Background Population*

For simulations modeling apparent visual magnitudes brighter than approximately 15.75, the MBA subset of the numbered asteroids with $V(a, 0) < 15.75$ (the "complete asteroid population") is the only required asteroid model. When the required limiting magnitude for a simulation is fainter than 15.75, the number of asteroids this model, or any set of orbital elements of known asteroids, would generate for a given area of the sky is less than the number that would actually be observed because of the incompleteness of the known population, thus the need for a "statistical" asteroid model.

In our analysis, we selected all 5983 asteroids through number 8603 not belonging to one of the 15 dynamical asteroid families discussed below. This sample was divided into four zones based on semimajor axes, as shown in Figure 1. Then, using the mean apparent visual opposition magnitude and albedos from the SIMPS (Tedesco et al. 2002) and from an Infrared Telescope Facility (IRTF) asteroid radiometry survey (Gradie & Tedesco 1988), the bias-corrected albedo distribution within each of these four zones was derived using the method described by Zellner (1979) and Tedesco (1979) and used to estimate the size distribution for asteroids in these zones for diameters down to 1 km.

Since one purpose of having albedos and diameters for all asteroids is to model their appearance on the sky as realistically as possible, assigning a single albedo to asteroids in each semimajor axis zone will not suffice. For example, in zone 2 (which contains 41% of the numbered MBAs) the bias-corrected fraction of low- and moderate-albedo asteroids is about equal (42% vs. 46%; Gradie & Tedesco 1982). If a single adopted albedo were used in this zone, the resulting distribution of albedos within the area of sky being simulated would be monomodal rather than, as known from the bias-corrected sample, strongly bimodal. Thus, we decided to group zones as described above, treat each separately, and assign albedos proportionately.

[5] Of the first 8603 numbered asteroids, 7729 are MBAs (2.064 AU $\leq a <$ 3.278 AU, $i < 25^\circ$, $e < 0.3$). Of these, 3810 have $V(a, 0) < 15.75$.

TABLE 2
COMPLETENESS DIAMETER (IN KILOMETERS) AS A FUNCTION OF ZONE AND ALBEDO CLASS

Zone	H	$\langle a \rangle$	Low	Int.	Mod.	High
2	13.12	2.30	14.19	9.98	7.06	4.71
3	12.28	2.66	20.85	14.74	10.42	6.95
4	11.81	2.89	25.79	18.23	12.90	8.60
5	11.38	3.13	31.48	22.35	15.74	10.49
4+5	11.50	3.06	29.76	21.05	14.88	9.92

We parameterized the albedos into four logarithmic mean albedo classes as shown in Table 1. These are simply the logarithmic means (-1.3, -1.0, -0.7, and -0.3) of each of the class ranges rounded to 0.05. This yields 0.05 for low-, 0.10 for intermediate-, 0.20 for moderate-, and 0.45 for high-albedo classes. The means (medians) for the four albedo classes from the nonfamily MBA sample are 0.0547 (0.0533), 0.0990 (0.0986), 0.1974 (0.1883), and 0.4624 (0.4364), respectively. Note that the low- and moderate-albedo classes include most of the C- and S-class asteroids, respectively, which dominate the MBA population.

Table 2 gives the absolute visual magnitude (H) as defined by Bowell et al. (1989) corresponding to $V(\langle a \rangle, 0) = 15.5$ (the highest magnitude bin for which the sample is complete), the mean semimajor axis ($\langle a \rangle$), and the completeness diameter for each zone and albedo class used in this study. Zones 4 and 5 are given both separately and combined because the distribution of albedos within each of these two zones was statistically indistinguishable, and so we combined them into a single zone designated "4+5."

These data were used to compute the bias-corrected albedo distributions given in Table 3, using the method described by Zellner (1979) and Tedesco (1979). That is, the proportion of asteroids within each albedo bin for asteroids lacking measured albedos is assumed to be the same as that for asteroids having such measurements. Because each albedo bin covers a restricted range of distances, is only 0.5 mag wide in $V(a,0)$, and contains no "special" classes of objects (such as family members) that might have been extensively observed as part of a special observing program, the objects in each bin are a random sample. The bias correction is necessary, because while the number of asteroids within a given zone and albedo class is assumed to be complete for $V(a, 0) < 15.75$ (i.e., virtually all asteroids brighter than this mean opposition magnitude have already been discovered), the diameter to which this corresponds varies within each zone according to the albedo, and, in turn, the fraction of the total number of objects belonging to each albedo class varies from zone to zone because of the well-known variation of asteroid albedos with mean heliocentric distance (Gradie & Tedesco 1982).

Radiometric albedos are available for ~48% of the nonfamily MBAs in the known asteroid module (see Table 4). We assigned albedos to nonfamily MBAs lacking such values as follows.

TABLE 3
OBSERVED/BIAS-CORRECTED ZONAL ALBEDO DISTRIBUTIONS (IN PERCENT)

Zone	Low	Intermediate	Moderate	High
2	35/42	6/5	52/46	7/7
3	49/53	5/8	43/37	3/2
4+5	72/74	6/7	20/18	2/1

TABLE 4
DATA USED IN ASSIGNING ALBEDOS AND DIAMETERS TO KNOWN ASTEROIDS WITH NUMBERS LESS THAN 8604

Data Source	Number in Source	Number Nonfamily	Number Family
SIMPS (Tedesco et al. 2002)	2006	1195	367
IRTF (Gradie & Tedesco 1988)	350	17	28
Family membership (Zappalà et al. 1995)	1877	0	907
Taxonomic class (Tholen & Barucci 1989)	959	51	1
$B-V$ color index (Tedesco 1989)	1017	32	0
Semimajor axis (MPC)	8603	1212	0

We considered the possibility that smaller asteroids might have systematically higher albedos due, e.g., to shorter collisional lifetimes, leading to a shorter exposure to space weathering. Therefore, we looked for albedo size dependences within each zone (cf. Tedesco 1994). We found that, with the exception of zone 3 and, to a lesser extent, zone 2, the albedo distributions for asteroids with diameters greater than 40 km and those smaller than this display no significant differences. For zone 2 the sample is too small to enable us to say anything definitive. There are only 65 asteroids in zone 2 with $D \geq 40$ km, and not many more will be found, as this is well above the completeness limit. For zone 3 the statistics are better; there are 215 asteroids in this zone with $D \geq 40$ km and over 300 smaller asteroids with radiometrically derived albedos. The albedo distribution for the larger asteroids in this zone is strongly bimodal, while that for the smaller asteroids is not. However, many of these smaller asteroids are below the completeness limit for this zone ($\sim$21 km for low-albedo asteroids and 11 km for moderate-albedo asteroids). Thus, because the *IRAS* sample is based on asteroids discovered at visual wavelengths, it is likely that the proportion of higher albedo asteroids for zone 3 in the $D < 40$ km sample is greater than in reality. If this is true, then ignoring it underestimates the number of small low-albedo asteroids in zone 3. For these reasons, we decided to make no distinction among asteroids based on their size.

Because the albedos used in this analysis are all based on infrared radiometry, it is important to know whether the albedos for small asteroids are accurate. Thus, we are conducting a polarimetry program to obtain independent albedo measurements for small asteroids having radiometric data. Preliminary indications are that there is no clear systematic difference between albedos derived from infrared radiometry and those obtained from polarimetry (Cellino et al. 1999a, 2005).

There are 2507 nonfamily MBAs with $V(a, 0) < 15.75$ among the first 8603 numbered asteroids. Of these, 1212 have radiometric albedos and diameters. Thus, nearly half (48%) of the nonfamily MBAs brighter than the completeness limit have measured albedos and diameters. An additional 83 have a measured $B-V$ color index or taxonomic class. Thus, over half (52%) either have a measured albedo or data from which an albedo can be inferred. See Table 4 for the details. We assigned albedos to nonfamily MBAs for which only an absolute magnitude and semimajor axis were available, using the results given in Table 3 as described below.

The procedure for assigning zone-based albedos to known asteroids lacking them and to the synthetic objects differed. The known asteroids in each zone were divided into "bright" [$V(a, 0) < 15.75$] and "faint" samples. Albedos were then randomly assigned to each asteroid in such a way that the bright sample, including those with measured albedos, matched the nonfamily MBA albedo distribution for the *complete* population, whereas the faint sample matched the *bias-corrected* nonfamily MBA albedo distribution (see Table 3).

This different treatment is necessary because the complete population is unbiased. The remaining, incomplete sample has no upper limit magnitude and is intended to be a diameter-limited sample. In practice, numbered asteroids with $V(a, 0) \geq 15.75$ are not used by SAM, since this population is modeled using the statistical models. The statistical background population models use the bias-corrected albedo distribution because they are intended to be "complete" to a limiting diameter rather than to a limiting mean apparent magnitude. Thus, the statistical background models assume that the albedo distributions given in Table 3 are correct and are the same for asteroids smaller than the bias-corrected sample, typically two or three diameter bins (each 0.1 in $\log D$) smaller than the completeness limit for each zone.

We adopted this approach so that the albedo distribution of the modeled asteroids would match, on a zone-by-zone basis, the complete or bias-corrected albedo distributions, as appropriate. This is a more realistic approximation than one using a single mean albedo for all asteroids in a given zone or one in which the albedo distribution is assumed to match that of the complete [$V(a, 0) < 15.75$] population.

For numbered asteroids, H, rather than diameter, is known from the orbital elements; thus, equation (1) was used, together with a statistically assigned albedo, to compute the adopted diameter:

$$\log(D) = 3.1236 - 0.2H - 0.5 \log(pV). \quad (1)$$

For the statistically generated asteroids the situation is the opposite, since the diameter is a priori "known" from the models used to generate the orbital distributions. Thus, for these a statistically assigned albedo and the "known" diameter were used in equation (2) to compute the corresponding H:

$$H = 15.62 - 5 \log(D) - 2.5 \log(pV). \quad (2)$$

The statistical background population models were created as follows. Cumulative SFDs for asteroids numbered through 8603, using diameters obtained as described above and containing only nonfamily MBAs ("background objects"), were created for each of the three semimajor axis zones. Then, as shown in Figure 2, these distributions were linearly extrapolated to 1 km, starting the fit near the last inflection point before (i.e., for diameters greater than) the completeness limit and ending near the smallest diameter in each zone for which each sample is supposed to be complete. The completeness diameter for each zone is the diameter for which H corresponds to $V(a, 0) = 15.75$ at the middle of the zone and with an albedo equal to the bias-corrected (i.e., weighted using the "complete" data from Table 3) mean albedo for that zone. Using this definition, the completeness diameters are 7, 12, and 20 km for zones 2, 3, and 4+5, respectively. These limits are shown as solid vertical lines in Figure 2.

This procedure gave populations of about 40,000 background objects larger than 1 km for zones 2 and 3 and about 70,000

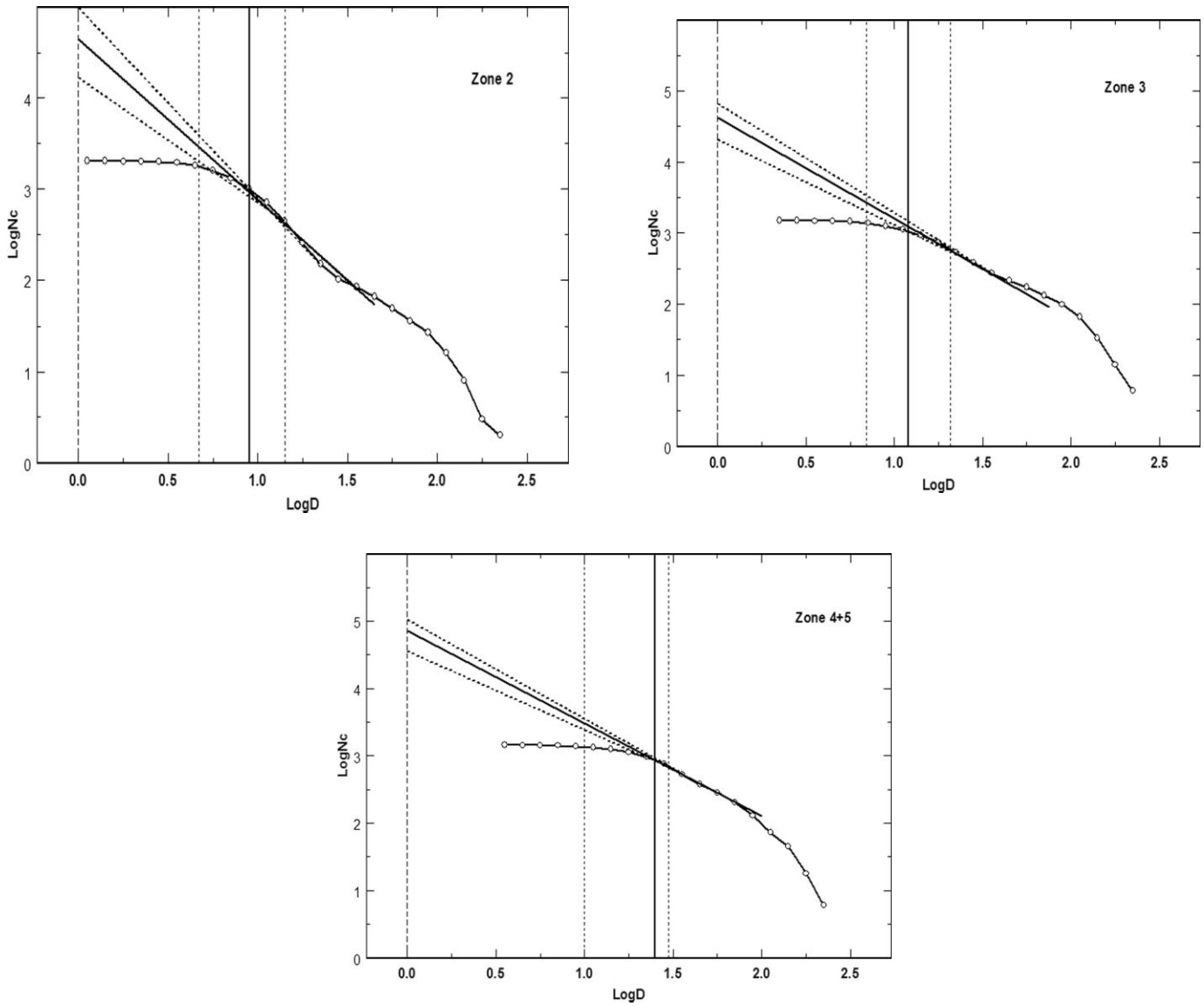

FIG. 2.—SFDs for background asteroids in zones 2, 3, and 4+5 extrapolated to 1 km. The dotted vertical lines bracketing the solid vertical line indicate diameters corresponding to low (*right*) and high (*left*) albedos (from Table 2), and the solid line corresponds to the bias-corrected logarithmic mean albedo at the center of each zone.

objects for zone 4+5. The uncertainties in these estimates, based on less plausible alternate extrapolations, are about 50%, as indicated by the steeper and shallower dotted lines bracketing the solid least-square-fit lines in Figure 2.

We next used these estimates to produce a file of synthetic background asteroids, one file for each zone, using a randomly generated diameter distribution matching that of the extrapolated cumulative distribution. Because we eliminated synthetic background asteroids larger than the nominal completeness limit (according to their generated albedo; see below and Table 2), and also because of some small rounding effects in the generation routine, the actual numbers of objects created in the three zones were 36,969, 37,675, and 67,943, respectively. In addition, numbered asteroids known to be smaller than the nominal completeness limit replaced (i.e., were substituted for) synthetic asteroids of the same diameter.

To each of these records we added orbital elements with uniformly distributed angular elements (argument of perihelion and longitude of the ascending node) matching the a, e, and i distributions of the sample of known asteroids in each zone having diameters above the completeness limit. The epoch of osculation for all elements is 1998 October 14 (JD 2,451,100.5). Next, albedos were randomly assigned to each record in proportion to their representation in that zone (i.e., the bias-corrected proportions given in Table 3). Finally, absolute magnitudes (H) were computed for each entry from its corresponding diameter and albedo using equation (2).

Table 5 gives the albedo distribution resulting from the procedure described above before elimination of the statistical background asteroids larger than the completeness limit. The concatenation of these three files constitutes the SAM's MBA background population model.

TABLE 5

STATISTICAL ALBEDO ASSIGNMENTS FOR THE NONFAMILY MBA STATISTICAL BACKGROUND MODEL

Population Group	Zone	Total No.	Low	Int.	Mod.	High
1.....	2	37822	15885	1891	17398	2648
2.....	3	38362	20332	3069	14194	767
3.....	4+5	68486	50680	4794	12327	685

TABLE 6
STATISTICAL ASTEROID MODEL FAMILIES

Family	D_C (km)	No. Known (N_K)	No. with $D \geq 1$ km (N_E)	No. Rej.[a] (N_R) (MB eject, escape e, $i > 90^\circ$, Mars crossing)	No. in SAM Database (N_T)
Adeona	17	63	100000	40 (9, 0, 0, 31)	99960
Dora	22	77	24000	11	23989
Eos	17	477	162000	58253 (36466, 21701, 0, 351)	103482
Erigone	10	45	16000	1408 (18, 0, 0, 1390)	14592
Eunomia	11	563	1000000	441165 (258935, 90244, 0, 91986)	558835
Flora	5	819	30000	12125 (8991, 1187, 0, 1947)	17875
Gefion	10	86	12000	21	11979
Hygiea	25	103	10000	5181 (4069, 693, 0, 419)	4819
Koronis	10	325	46000	10738 (3095, 7639, 0, 4)	35262
Maria	9	120	21000	5591 (2900, 2368, 0, 323)	15409
Massalia	8	49	100000	2	99998
Merxia	11	26	2500	3	2497
Themis	20	550	1000000	542767 (431151, 65569, 0, 46047)	457233
Veritas	28	22	6000	236 (236, 0, 0, 0)	5764
Vesta	6	231	350000	63384 (42350, 15336, 0, 5698)	286616
Totals			2879500		1738310

[a] The number of statistically generated objects rejected because they were immediately ejected from the main belt (2.1 AU $> a >$ 3.3 AU), had an eccentricity that would result in their eventual escape from the main belt, had an inclination $>90^\circ$, or became Mars or Jupiter crossers. (The Jupiter-crosser possibility, although included for the sake of completeness, never occurred, but the first, ejection from the main belt, is frequent in the inner belt.) The actual values for the orbital elements generated depend on the seed used in the simulation's random number generator, but their distribution is very weakly dependent on it.

In practice, the known asteroid module includes all MBAs with $V(a, 0) < 15.75$, including numbered members of asteroid dynamical families. This known asteroid module is then combined with the three background population models, described above, and the 15 dynamical asteroid family models, described below. This set of H, G, diameter, albedo, and orbital elements for the complete asteroid population and the 18 population models together constitute the SAM that can be used to create the SFD, and to simulate the sky plane distribution, of MBAs with diameters $\geq$1 km.

2.2. *The Families*

As noted above, we decided to separately model MBAs belonging to a number of the most prominent dynamical families identified by Zappalà et al. (1995). The list of families used is given in Table 6, where we identify each family by the name of its lowest numbered member (which is also, in most cases, the largest family member).

Table 6 also gives for each family the completeness diameter (D_C, the size above which the population of each family is thought to be complete), the number of known family members (N_K) from Zappalà et al. (1995), the cumulative number of objects (N_E) larger than 1 km predicted by the family size distribution model of Tanga et al. (1999), the number rejected (N_R) using the velocity model (see below), with the corresponding reason(s) for the rejection, and the total number in the SAM database (N_T), where $N_T = N_E - N_R$, i.e., N_T includes the N_K asteroids contained in other modules, e.g., family asteroids with $V(a, 0) < 15.75$ from the known asteroid module and known family members with diameters less than D_C, which were substituted for nonrejected statistical asteroids of the same diameter.

We did not use all of the "robust" families found by Zappalà et al. (1995), because in several cases some families overlap each other in a very complicated way in orbital proper element space. In these cases, the nominal memberships of adjacent families are mostly tentative, in the absence of a spectroscopic data set large enough to allow us to distinguish the members of different groupings. This is particularly true for the families found in the middle region of the main belt, where complicated groupings (the "Lydia complex," including the families of Lydia, Nemesis, Liberatrix, Henan, and Taiyuan) are located. Even after the excellent spectroscopic work of Bus (1999), who was able to discriminate among different family memberships in a number of interesting cases, the situation is still such that no reliable extrapolation of the size distributions is possible. In addition, some families were discarded because of the very small number of known members, like the Chloris and Meliboea families. In these cases also, any extrapolation of the number of members to small sizes is meaningless. In any case, these groupings are irrelevant from the point of view of the asteroid inventory for $D > 1$ km because their largest members are so small that their contribution to the total population is negligible. This conclusion also applies to most of the families that were not used because of their uncertain memberships, like the above-noted Lydia complex.

The only case in which we were forced to discard a family that might be of some relevance to the question of the overall asteroid population is that of the Nysa family. This is a populous family, composed of nearly 400 objects according to Zappalà et al. (1995). The problem is that this family consists of two distinct subgroupings, named Mildred and Polana by Cellino et al. (2001), that are probably overlapping only by chance and that cannot be easily separated. Under these conditions, any extrapolation of the supposed number of members to small sizes would be very uncertain, although some recent spectroscopic observations (Cellino et al. 2001) may allow us to make reliable predictions in a future version of our model.

We note also that in some cases (Flora, Eunomia, and Maria) we enlarged the nominal member lists by including objects classified as "Quality Code = 1" members by Zappalà et al. (1995). The reason is that in these cases we knew from previous analyses (e.g., Migliorini et al. 1995) that the nominal member lists are too conservative. Moreover, our Gefion family corresponds to the Ceres family found by Zappalà et al. (1995), after removing the very likely interlopers 1 Ceres, 255 Oppavia, and 374 Burgundia.

What is important here is that the size distributions of the families obtained from the average albedo and the observed absolute magnitudes of their members are power laws characterized by very steep slopes (Cellino et al. 1991; Tanga et al. 1999). These slopes, much steeper in general than those of the typical background asteroid population, may mean that family asteroids dominate the population at small sizes (Zappalà & Cellino 1996). It is for this reason that we decided to treat family and nonfamily asteroids separately.

Some caveats with this approach should be pointed out. First, as mentioned above, there are indications that below the size of completeness many families might have shallow SFDs (Morbidelli et al. 2003). These conclusions are based on analyses of the SDSS results and if confirmed should certainly be taken into account in a future version of our model. However, as discussed by Cellino et al. (2004), the debate is still open on this subject, mainly because of the discrepancy (approximately a factor of 3 in the estimated number of MBAs with diameters >1 km) between the SDSS results and findings from surveys carried out at thermal infrared wavelengths (see also below).

Second, the populations of the families in Table 6 were derived using the results of Tanga et al. (1999), modified as described in the following paragraph. In particular, these authors were able to fit the observed family size distributions by means of a model taking into account geometric constraints in the collisional origin of the members as fragments of parent bodies of finite sizes. What is more important in the present context is that this approach allows us to make extrapolations of the size distributions down to 1 km. It is nearly certain that at some poorly determined diameter, the steep power-law trends of these distributions must relax to more moderate values (Marzari et al. 1995). However, Tanga et al. (1999) showed that an extrapolation down to 1 km should be reasonable and reliable in most cases. Actually, some families are already complete down to a few kilometers in size (see D_C in Table 6), indicating that an extrapolation to 1 km should be reasonably reliable.

Nevertheless, it is clear that at least some of our extrapolations are uncertain. This is particularly true, for instance, in the case of the Hygiea family. This is likely an old grouping (see Tanga et al. 1999) with only a few objects, including several plausible interlopers, larger than the completeness limit. For this family, any extrapolation of the size distribution must be considered tentative. However, since this family contributes only about 2% to the total MBA population for $D > 1$ km, this is not a significant problem. Thus, the extrapolated number of objects given in Table 6 represents a compromise of different possibilities, compatible with the data at our disposal. Since we are aware of several objections that could be raised concerning our treatment of families, we have also explored different scenarios, as is mentioned below.

While the albedo distributions of families are simpler than those of nonfamily (background) asteroids, their orbital distributions are somewhat more complex. This is because family asteroids are not located randomly in orbital element space within a given region. Instead, family members are fragments from collisional events that were ejected from the parent body with a distribution of ejection velocities. In particular, this problem was analyzed by Cellino et al. (1999b), who found that a general relationship exists between the maximum possible ejection velocities of fragments as a function of their sizes. Moreover, events characterized by different impact energies lead to differences in the parameters describing the size-velocity relation.

In this respect, we note that recent studies (Michel et al. 2001; Bottke et al. 2002; Nesvorný et al. 2002) suggest alternative explanations for the observed size-dependent spreading of families in orbital element space. In particular, the above authors are convinced that these properties are not directly related to the kinematical properties of the original ejection velocity fields of the fragments in family-forming events but argue instead that they are mostly the result of a postformation evolution, driven primarily by dynamical evolution under the influence of the Yarkovsky effect. This subject is also extensively discussed by Cellino et al. (2004). For the purposes of SAM, this issue is not too important, because our modeling of families is based on empirical fits to the observed distributions, regardless of the physical mechanisms that produced the size-dependent spreading of families that we observe today.

In the present paper, the size-velocity relation for each family has been modeled using a code that creates synthetic fragments ejected according to the observed distribution for the members of each family in orbital proper element space. In particular, smaller fragments are assumed to be located at increasingly larger maximum distances from the family barycenter, according to the results of Cellino et al. (1999b). In order to avoid unrealistically high reconstructed ejection velocities, the maximum allowed distance of the fragments in the simulation of each family is not simply computed on the basis of a mechanical extrapolation of the observed size-ejection velocity relation but is limited to values not significantly exceeding those of the most distant (and smallest) members observed in each real family. In this sense, by having a priori limited the maximum distances achievable by the smallest fragments generated in our simulations to values close to the maximum observed for each family, we have increased the reliability of the simulated families. This degree of sophistication is not crucial for the limited purposes of the present paper, since, for the most part, family members remain clustered within a limited region of orbital element space (around the family "barycenter"). However, in a number of cases (indicated in Table 6) the smallest fragments in our simulations turned out to be ejected at speeds sufficient to achieve orbits with semimajor axes outside the borders of the main belt and/or into Mars-crossing orbits. Mars-crossing orbits are known to lead to fast dynamical evolution into near-Earth orbits (Migliorini et al. 1998). For each of these cases, we discarded the N_R resulting fragments and subtracted them from the resulting family file; the final column in Table 6 (N_T) gives the total number of these asteroids in SAM.

Note that our procedure for the creation of synthetic family members as explained above reflects the epoch when this analysis was started. Currently, several objections can be raised regarding this procedure based on subsequent findings, primarily regarding the role of the Yarkovsky effect. In particular, major objections can be raised regarding our assumptions that (1) a steep size distribution characterizes current families at small sizes and (2) the present spreading of families in orbital proper element space is diagnostic of the original ejection velocity distributions of family fragments.

Point (1) is related to the fact that many small family members would have disappeared because of a Yarkovsky-driven semimajor axis drift, leading the objects to eventually cross a nearby region of chaotic motion from which they are ejected from the main asteroid belt. Moreover, the collisional evolution of members of families some gigayears old also leads to a relaxation of the SFDs (Marzari et al. 1995). Point (2) is also related to the Yarkovsky effect, since it is likely that the original ejection velocities of family fragments were much lower, as also suggested by results of hydrocode simulations by Michel et al. (2001), and the current spreading of families in the orbital proper element space could be mostly due to a Yarkovsky-driven evolution.

TABLE 7
SAM Asteroid Family Mean and Median Albedos and Standard Deviations Obtained from Radiometric Observations

Family	*N*	Mean Albedo	Median Albedo	Sigma	Remarks
Adeona	13	0.0734	0.0739	0.0205	1384 Kniertje, 0.3077, rejected before analysis
Dora	12	0.0603	0.0585	0.0160	7083 Kant, 0.1161, rejected by Chauvenet's criterion
Eos	100	0.1359	0.1329	0.0426	423 Diotima, 0.0515 C, and 283 Emma, 0.0262 P, rejected before analysis and 677 Aaltje, 0.2794, and 1186 Turnera, 0.2919, rejected by Chauvenet's criterion
Erigone	5	0.0569	0.0580	0.0123	
Eunomia	36	0.1494	0.1397	0.0864	Broad distribution with a strange mix of taxonomic classes. Webb, 0.6110, rejected by Chauvenet's criterion.
Flora	47	0.2113	0.2301	0.0905	422 Berolina, 0.4930 E, rejected before analysis and 341 California, 04950, rejected by Chauvenet's criterion
Gefion	6	0.0824	0.0473	0.0738	Bimodal?
Hygiea	10	0.0515	0.0527	0.0141	108 Hecuba, 0.2431 S, and 100 Hekate, 0.1922 S, rejected before analysis and 867 Kovacia, 0.0923, rejected by Chauvenet's criterion
Koronis	26	0.2094	0.2087	0.0603	Clean, tight distribution
Maria	18	0.2224	0.2309	0.0525	Clean, tight distribution
Massalia	1	0.2096	...	0.0603	Used same sigma as for the Koronis family, which has a similar albedo
Merxia	1	0.2207	...	0.0603	Used same sigma as for the Koronis family, which has a similar albedo
Themis	134	0.0834	0.0830	0.0338	
Veritas	6	0.0693	0.0726	0.0150	Clean, tight distribution
Vesta	3	0.2870	0.2800	0.0795	442 Eichsfeldia, 0.0386 C, rejected before analysis. Used 0.3698 for Vesta's albedo.[a]

[a] This (0.3698) is the albedo corresponding to the occultation diameter (500.7 km; Dunham 1992). There is also radiometric data: a TRIAD albedo (0.316 converted to the IMPS system) and a single measurement (0.361) from Gradie & Tedesco (1988). The SIMPS result (0.4228) is considered suspect.

Taking into account these two possible objections, we have performed some different simulations, characterized by the following differences with respect to the procedure described above: (1) we made extrapolations of the size distributions of families using a shallower, Dohnanyi-like SFD below the completeness size of each family; (2) we considered lower limits for the maximum possible ejection velocity, preventing the objects from achieving unrealistically high velocities capable of removing them from the family neighborhood; and (3) we introduced a "Yarkovsky depletion effect." Only 10% of family fragments having a size of 1 km can still exist, and we linearly scaled this depletion mechanism so that 90% of the fragments having a size of 9 km still exist as identifiable family members. Obviously, the above values used to characterize the Yarkovsky depletion are arbitrary. In addition, we made these tests for only a couple of families (Eunomia and Koronis) as a check of what would happen if we modified our simulation in order to use a more modern approach, better suited to the current "Yarkovsky era."

The result of the exercise above is that the final number of family members does not change significantly with respect to the older, "pre-Yarkovsky" model. The reason for this is that different mechanisms have different effects on the resulting families. Assuming a Dohnanyi-like size distribution causes the number of small family members to decrease. This obvious effect is more than compensated by the fact that the lower ejection velocities prevent large numbers of small fragments from being removed from the family neighborhood (no resonance crossings occur, etc.). However, adding a Yarkovsky depletion effect produces a total number of family members that is not essentially different from the original families created by the "pre-Yarkovsky" code.

Although we have performed only a very limited test, it is clear that a future version of our model can include changes in the generation code, as described above, to produce more realistic families. Thus, based on the results of these preliminary tests, we believe that the current version of SAM yields reasonably accurate results.

While the inventory and location of family members in the orbital proper element space present a number of technical problems, as we have seen above, in some other respects families are easier to model than the background population because, as a general rule, family albedo distributions are fairly homogeneous (Cellino et al. 2002). To date, no case of well-defined albedo variegation among members of the same family, possibly reflecting an origin from a differentiated parent body, has been clearly demonstrated.

The mean albedos and standard deviations for the families used in this study were determined as follows. Only family members with an albedo derived from a radiometric observation were used. Next, this set of data was examined for taxonomic classes that would be inconsistent with those of the other family members. Finally, the mean albedo and standard deviation were computed, and Chauvenet's criterion[6] (Chauvenet 1863) was applied once. The results of this procedure are given in Table 7.

The observed mean albedo and its standard deviation for each family are assumed to be representative of the entire family. This is a reasonable assumption because the albedo distributions for members of all 15 families being considered here are rather narrowly distributed. With the exception of the Massalia and Merxia families, for which only one measured albedo exists, all families have at least five members with a measured albedo, and two have $\geq$100. Thus, albedos were randomly assigned to each of the synthetic asteroids such that the mean and standard deviation for the synthetic sample matched that of the sample with measured albedos. Next, the absolute visual magnitude (H) for each of the statistical family asteroids was computed from the diameter (D), in kilometers, and albedo (p_V) via equation (2). All statistical

[6] A procedure for identifying outliers in data sets; see Taylor (1982) for further details.

asteroids were assigned the default value of 0.15 for the slope parameter (G)[7] needed to compute apparent V magnitudes of the objects at any given epoch (and corresponding phase angle).

The synthetic families generated by our code are interesting per se, showing that family forming events have likely been responsible for some mixing of different taxonomic classes at small sizes and have had consequences for the generation of near-Earth objects (in agreement with Zappalà et al. 1998). However, these topics are certainly model-dependent and beyond the scope of this paper and will be treated in future publications.

3. STATISTICAL ASTEROID MODEL: THE DATABASE

The SAM database consists of two files: a "Known Asteroid Module" file (295,481 bytes) and a "Statistical Asteroid Module" file (171,163,107 bytes). Both files are available from the NASA Planetary Data System's Asteroid Archive.[8] Asteroids in the known asteroid module, not belonging to one of the 15 asteroid families used here, had their diameters and albedos assigned as described for the background module (see Table 4 for the details).

The total number of "statistical" family members is 1,738,310. To this were added the 142,587 statistical "background" model asteroids and the 3810 asteroids from the known (complete) MBA module, bringing the total number of asteroids in SAM to 1,884,707.

Figure 3 gives the cumulative diameter frequency distribution for SAM. The lower curve is that for asteroids from the known MBA module with numbers <8604, i.e., the data set from which SAM was created. Superposed on this, as open squares, is the cumulative diameter frequency distribution using all the diameters from the known and statistical asteroid modules. The heavy curve through the open squares is a third-order least-squares polynomial, given in equation (3), fit to the data with $0.0 \leq \log D \leq 2.0$:

$$\log N_C = 6.275 \pm 0.013 - (3.214 \pm 0.056)(\log D) + (0.974 \pm 0.066)(\log D)^2 - (0.182 \pm 0.022)(\log D)^3. \quad (3)$$

From the figure it is apparent that the SAM SFD for the entire main belt contains no abrupt slope changes below the completeness diameter of 36.16 km ($\log D = 1.56$). The large separation between the vertical dashed lines for the diameter completeness limits at the inner and outer edges of the main belt illustrates the sensitivity of the diameter completeness limits to distance and albedo.

Whereas the agreement regarding the total population with diameters greater than 1 km is within a factor of 2.6 with the most recent observations (see below), an extrapolation of SAM to 100 m using equation (3) results in a discrepancy between SAM and, e.g., DGJ98, of a factor of 760, viz., 44 billion versus 58 million, respectively. We do not advocate using equation (3) to extrapolate SAM to smaller sizes.

4. COMPARISON WITH DATA AND OTHER MODELS

4.1. *Uniqueness and Reliability*

SAM is statistically correct but not unique. Even above the completeness limit, there are numerous asteroids lacking physical observations, or even a family membership, with which to constrain their diameters. Hence, individually, these estimated diameters are of little use for most purposes. However, taken collectively they reproduce the albedo distributions for asteroids with known albedos in each of their population groups (family or background zone) because they were created to do so.

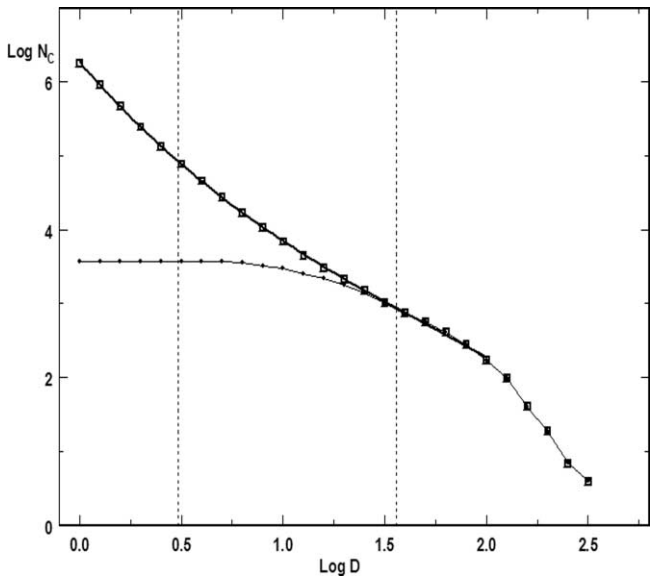

FIG. 3.—SAM cumulative diameter frequency distribution. The lower curve indicates the distribution using the numbered asteroid data set for numbers <8604. The open squares are the entire SAM data set and the heavy curved line shows a least-squares third-order polynomial eq. (3) fit to the SAM data set for $\log D \leq 2.0$. The vertical dashed lines indicate the diameter completeness limits at the inner (*left*, $a = 2.064$ AU) and outer (*right*, $a = 3.278$ AU) edges of the main belt.

The overall reliability of SAM depends on the veracity of the assumptions used in creating it. Although we are convinced that these assumptions constitute a reasonable treatment of the problem making the best use of the available data (or, to be more precise, of the data available at the beginning of the present analysis), it is clear that only observations can be used to support or reject the model. Our procedure, explained in detail in § 2, makes two assumptions: (1) Asteroids lacking physical observations have the same albedo distributions as asteroids in similar orbits, and within a 0.5 mag bin in mean opposition magnitude, having such data; and (2) the albedo distribution for asteroids with diameters far below the (semimajor axis dependent) completeness limit is the same as that for asteroids above this limit but with a sufficient number of asteroids having measured albedos from which to obtain an albedo distribution. Having an albedo for each of the known asteroids allows us to use their H magnitudes to compute a diameter. This then allows us to create $\log D$- $\log N$ plots for each of the 18 population groups, for each of which the diameter completeness limit is known. The third and final assumption is then made: the extrapolation for each of these groups from the diameter completeness limit to 1 km is as described in §§ 2.1 and 2.2. Obviously, abrupt changes in the slope of the SFD for some families between 1 km and the current completeness diameter are possible, as extensively discussed above. However, SAM is a statistical model, and we are confident that the extrapolations performed for background and family population groups are reliable in a statistical sense.

The ultimate assessment of the correctness of the above assumptions must come from observations. That is, SAM can be used to predict the numbers, distribution among the 18 population groups, apparent motions, and fluxes of MBAs at any given

[7] The known asteroid module includes 98 asteroids with a slope parameter $\neq 0.15$.

[8] See http://www.psi.edu/pds/SAM-I.

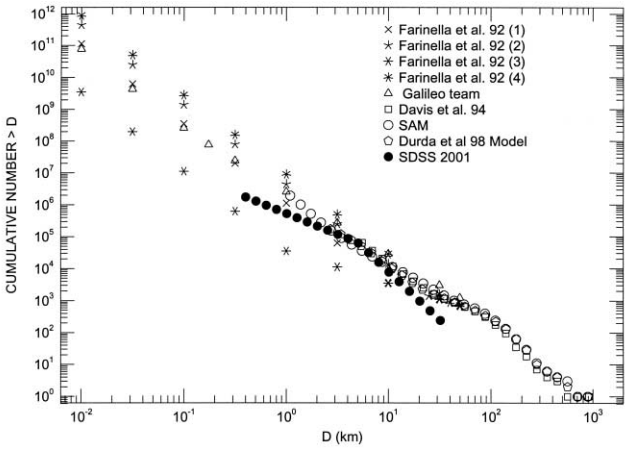

FIG. 4.—Model MBA SFDs (adopted from Davis et al. 2002; "Galileo team" = Belton et al. 1992).

wavelength in any given field for a given epoch. An observational test of the model is then conceptually and technically simple, although it is challenging in practice because of the need for space-based infrared observations and large ground-based telescopes for near-simultaneous (i.e., within ± 1 week) visual observations, not to mention scheduling issues arising from the need for coordinated infrared and visual observations.

4.2. *Comparison with Existing Observations*

Currently, there are only two published population estimates to compare with SAM's: the Ivezić et al. (2001) investigation based on preliminary SDSS data, and the Tedesco & Désert (2002) *ISO* Deep Asteroid Search (IDAS). Each of these studies gives an estimate of the MBA population for diameters greater than 1 km. These estimates differ by a factor of 2.6. Neither of these studies was designed to test SAM, and neither contains the information required for a true test of SAM. Nevertheless, these studies provide useful information as discussed below.

The first available observational test at visual wavelengths is provided by the recent SDSS study. As shown in Figure 4, the SDSS-derived size distribution is below the SAM prediction for a size of 1 km. Perhaps more importantly, the shape of the SDSS SFD is significantly different from that of the SAM SFD. If the SDSS SFD is correct, then SAM overestimates the MBA population above 1 km by a factor of 2.6.

The IDAS study, the first available observational test at infrared wavelengths, using maps at 12 μm, found 160 ± 32 asteroids deg^{-2} with 12 μm flux densities greater than 0.60 mJy. This is substantially in agreement with the SAM prediction (190 ± 20) for the same date, wavelength, observing geometry, and sensitivity limit as the actual observations.

The SDSS and IDAS studies each have their own limitations, discussed in their respective publications, and probably contain unrecognized systematic errors as well. Nevertheless, regarding the total population with diameters greater than 1 km, they are in agreement with SAM to within less than a factor of 3. Additional observational tests are certainly needed; one (SKADS; see § 5.2) has already been conducted, and others are being planned.

4.3. *Comparison with Existing Data and Models*

Figure 4 shows how SAM compares with seven other recent asteroid SFD estimates. As demonstrated in the figure, SAM is a middle-of-the-road model for diameters larger than 1 km in that SAM's total population is around the middle of those given by the models plotted (and cited) in this figure. The Farinella et al. (1992) model 3, and possibly model 4 as well, the lowest and highest in the figure, are ruled out by recent observations (Ivezić et al. 2001; Tedesco & Désert 2002). This leaves the Farinella et al. (1992) model 2 and SDSS (Ivezić et al. 2001) distributions as the current extremes.

It is generally accepted that over 95% of non-NEAs with $V(a, 0) < 15.75$ have already been discovered (see, e.g., Zappalà & Cellino 1996; JM98). Actually, it is likely that, through early 2002, over 98% of these bright MBAs have been discovered. For example, the 2002 April 21 daily orbital element file available from the MPC),[9] hereafter referred to simply as the MPCOrb file, contains elements for 149,940 MBAs:[10] 37,873 numbered, 84,544 multiapparition, and 27,523 single apparition. Of these, 4366 MBAs (using the inner, middle, and outer regions defined by JM98) have $V(a, 0) < 15.75$. However, more significantly, of the last 10,000 asteroids added to each of these three groups, only 34, two, and zero, respectively, have $V(a, 0) < 15.75$. Thus, even if there are as many as 4500 MBAs with $V(a, 0) < 15.75$, 97.0% have already been discovered. It is unlikely that there are an additional 134 MBAs with $V(a, 0) < 15.75$ lurking among those still awaiting discovery.

Using a given definition for the main belt or its subdivisions, one can study the absolute magnitude (H) distribution of the asteroids without further ado, but if one is interested in the distribution of the sizes, then a size, parameterized as the diameter (D) in kilometers here and in the study of DGJ98, is required for each MBA. Diameters can be obtained in several ways ranging from actually measuring them to estimating them by using an assumed albedo (p_V) to compute them from H via equation (1). In practice, a mixture of measured and estimated diameters is used, since measurements are available for only a small and rapidly shrinking fraction of the known asteroids.

Because the SAM population model was created using data for 8603 numbered asteroids and the JM98 work is of a similar vintage, comparison of these distributions with the MPCOrb distribution, in principle, tests how well these two models represent the true population. For values of H brighter than the completeness limit, the MPCOrb distribution defines the "true population," and for values of H fainter than the completeness limit, the MPCOrb distribution sets a lower limit on the true population. Figure 5 presents plots of absolute magnitudes versus cumulative numbers for five different data sets.

The values of H for all main-belt MPCOrb asteroids, only those numbered through 8603, and the SAM model for $H < 11.5$ are all essentially from the known main-belt asteroid module and are therefore not a test of SAM, since this population is complete. The dotted line in Figure 5 is offset 0.5 mag from the MPCOrb curve to avoid overlapping with the other curves and yet provide some indication of the magnitude of the effect of a probable systematic error in H discussed below.

The open squares and solid line in Figure 5 for $H > 11.5$ are, respectively, the SAM and JM98 models of the H distribution. These can be compared with one another and with the sample of known MBAs as of early 2002 (*top set of dots*). For $11.5 < H < 14.0$, the MPCOrb sample and SAM are well represented by essentially parallel straight lines with linear correlation coefficients of 0.9997 and 0.9977 and slopes of 0.50 ± 0.01 and 0.51 ± 0.01, respectively. The JM98 curve is nonlinear and mostly higher than SAM. Because of this curvature of the JM98

[9] See http://cfa-www.harvard.edu/iau/mpc.html.

[10] Using the definition of JM98: 2.0 AU $\leq a \leq$ 3.5 AU, $e \leq 0.40$, $0^\circ.5 \leq i \leq 45^\circ.5$.

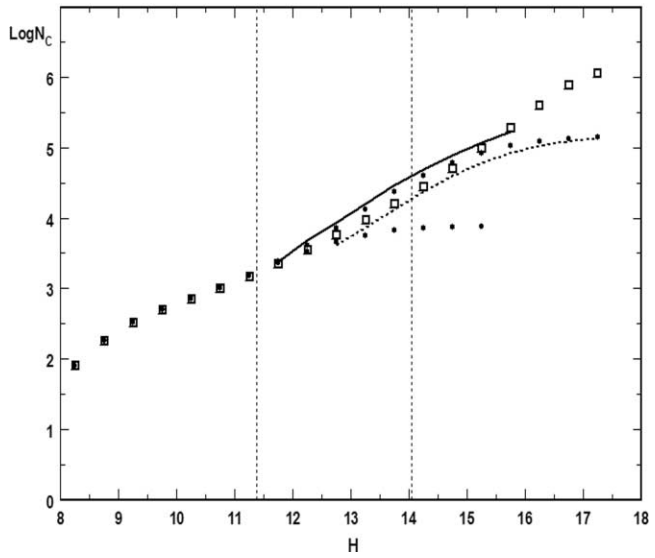

FIG. 5.—Absolute magnitude (H) vs. log cumulative number. The top set of dots is the H distribution for all main-belt MPCOrb asteroids, and the bottom set of dots is that for those numbered through 8603. The dashed curve between the two sets of dots shows the top set shifted 0.5 mag to the right. The open squares are the SAM model. The dashed vertical lines shows the values of H corresponding to $V(a, 0) = 15.75$ at the inner (*right*) and outer (*left*) edge of the main belt. The solid line at the top indicates the JM98 cumulative distribution for $11.75 \leq H \leq 15.75$, the range common to all three of their regions.

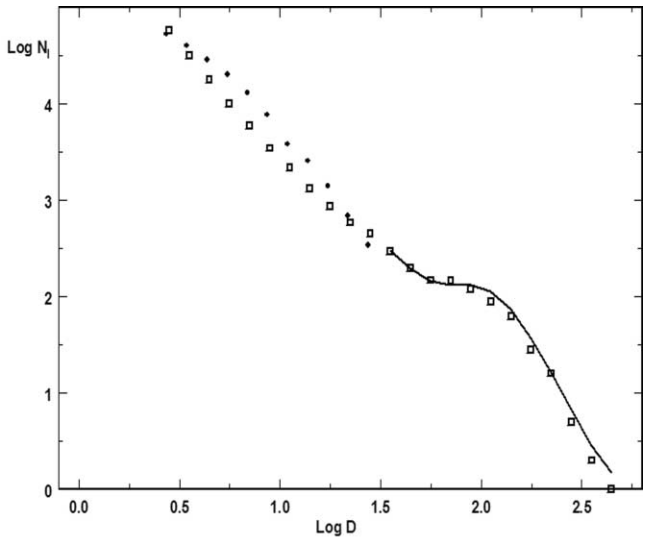

FIG. 6.—The $\log D$ vs. $\log N_I$ incremental number distributions for the SAM and DGJ98 models. The open squares are for the SAM.

curve, SAM begins to predict larger numbers of objects at fainter magnitudes. Curiously, the known MPCOrb asteroid sample is higher than SAM for $H < 15.0$. This is likely due to the aforementioned probable systematic error in H.

Actually, comparison of the MPCOrb H distribution with other distributions is of limited value because of systematic errors in MPCOrb's values of H. To make matters worse, this error is greatest for the higher numbered and unnumbered asteroids, the very ones we need to test the various models. See § 3.2.1 of Jurić et al. (2002) for a discussion of this particular issue and Jedicke et al. (2002) for a broader treatment of issues regarding asteroid orbital element databases. The relevant finding, for the present discussion, by Jurić et al. is that they have convincingly demonstrated the existence of a systematic error in the values of H in the MPCOrb file; i.e., that for the higher numbered and unnumbered asteroids, the MPCOrb H values are ~0.2 mag too low. In addition, they also demonstrated a systematic difference between the MPCOrb H values and Lowell Observatory's AstOrb element database,[11] the element database used in their study.

The systematic error in the MPCOrb H values is, presumably, present only for the higher numbered and unnumbered asteroids, but the place in the file where this error begins, and how much overlap exists between the valid and invalid H records, is unknown. Thus, we cannot simply add 0.2 mag to all the MPCOrb H values or even a subset of them. Eventually we will be able to statistically correct for this offset. However, as can be seen in Jurić et al's. (2002) Figure 7, H values derived for the lower numbered asteroids, based primarily on magnitudes obtained from photographic plates, are accurate to within about 0.2 mag, whereas the remainder, based almost entirely on magnitudes obtained using CCD imagers, are only precise to about twice this value. It is well beyond the scope of the present paper to discuss this issue any further, so in closing we note that observers using photographic plates apparently produced better magnitudes than those using CCD imagers, something only partly due to the fact that a typical photographically observed asteroid was several magnitudes brighter.

A systematic error in the MPCOrb H values, as described above, is also required to reconcile the H distribution for the known asteroids with that of the JM98 model. This is due to the fact that, in the absence of a systematic error in H, the JM98 model is a good fit to the *current* MPCOrb data, which are, by definition, incomplete below the completeness limit.

Turning next to a comparison of diameter distributions, we compare SAM to the DGJ98 model in which they took the JM98 results, transformed them to diameters, and used the resulting SFD for $D \geq 3$ km as the basis for their strength-scaled collisional model. Figure 6 gives the SAM and DGJ98 $\log D$ versus $\log N_I$ (i.e., incremental number) distributions. Given the caveat below, the two models are in substantial agreement for $\log D \geq 1.5$. However, for $\log D < 1.5$ the DGJ98 "observed" SFD is convex, whereas the SAM distribution is concave. Some of this difference is due to the different ways in which the data have been binned, but we believe the majority is caused by the different ways in which the diameters for $\log D < 1.5$ were estimated, i.e., by DGJ98's assumption of a single mean albedo for all asteroids with $D < 30$ km (actually, for $\log D < 1.5$, the small-size end of the solid curve in Fig. 6).

The shape of the SFD is important, since this is related to the properties of the overall collisional regime. In particular, a low-size cutoff produces a wavy structure that propagates through the size distribution (Campo Bagatin et al. 1994). This wave structure has been interpreted in terms of strength properties in past studies (DGJ98). If SAM is an accurate approximation of reality, this idea may need to be revised. However, it appears to us that the first priority should be to better define the observed SFD, and future versions of SAM provide one means by which to do this. If real, the lack of a wave structure in SAM may be due to its suppression by the violent events that create the asteroid families that dominate the SAM population at small sizes.

Both of the comparisons above are complicated by the fact that JM98 and DGJ98 used different H and D bins than SAM and a different definition of "main belt." This fact notwithstanding, the comparisons presented here serve to demonstrate that these

[11] See ftp://ftp.lowell.edu/pub/elgb/astorb.html.

TABLE 8
EXAMPLE ASTEROID SURVEYS

Name	Primary Wavelength (μm)	Assumed Brightness Limit	Total Area Surveyed (deg^2)	Approx. Solar Elongation (deg)
NESS	0.6	$V = 21.0$	980	45–70
SKADS	0.7	$V = 25.0$[a]	8.6	180
SDSS	0.36–0.89	$V = 22.5$	500	180
IDAS	12.0	0.60 mJy	0.06	106
FLS-EPC	8.0	0.06 mJy	0.13	115

[a] The actual limiting magnitude achieved was closer to 24 (Davis et al. 2004).

recent models, while in general agreement, have some significant differences. They also serve to demonstrate that the SAM absolute magnitude and diameter distributions are in general agreement with previous estimates, and, being based on an accurate analysis of the currently available albedo data, we believe they are already sufficiently close to the "true" distributions to be useful. This usefulness takes several forms, e.g., (1) serving as the boundary condition for models of collisional evolution, (2) simulating the sky-plane distribution for observational programs, and (3) for using existing and new observations to refine the current model and extend it to smaller sizes.

5. APPLICATIONS

Because SAM can be used to estimate asteroid positions and fluxes for any given date, it makes an ideal planning tool. Simulations can be used as an aid in planning and interpreting observations. Orbital element sets for known asteroids can provide some of this information, such as rates of motion, but because of the severe albedo bias of the known population above $V(a, 0) \sim 15.75$ (i.e., at diameters below $\sim$7–20 km), they will not give realistic estimates of how many asteroids will be in the field above the limiting sensitivity for deep surveys or provide reasonable estimates of the distribution of distances, diameters, albedos, or magnitudes for asteroids within the field.

Below we present examples of several kinds of surveys that can benefit from, and contribute to the development of, the SAM. These include a space-based visual wavelength near-Sun survey, two ground-based visual wavelength near-opposition surveys, and two space-based ecliptic plane surveys at wavelengths of 8 and 12 μm. These surveys are summarized in Table 8. As we discuss below, one of these surveys (IDAS) is published, as are preliminary results from another (SDSS). The data for the SKADS survey have been obtained (Davis et al. 2004) and, at the time this paper was submitted, the NESS and *Spitzer* First Look Survey-Ecliptic Plane Component (FLS-EPC) programs were being planned.

The purpose of these examples is to explicate the usefulness of SAM and not to compare the relative merits of these surveys. In addition, results available by using the orbital elements for known asteroids (e.g., motion vectors), although derivable from SAM, are not discussed in any detail in this section. See Figure 4 for how SAM compares with other published SFDs.

Because the current version of SAM does not contain any Earth-approaching, Mars-crossing, Hungaria, Phocaea, Cybele, Hilda, or Trojan asteroids, it is seriously incomplete for certain kinds of simulations. For example, the lack of Trojans will cause the sky-plane density of asteroids at 70 μm to be significantly underestimated, and the absence of Phocaeas and Hungarias will result in an underestimation of the confusion introduced into searches for near-Earth objects at small solar elongations.

Furthermore, in doing these simulations it became apparent that a 1 km diameter limit is insufficient to simulate the MBA population in fields as close to the Sun, or for the sensitivity limits, as used in the examples given here. Thus, we extended the original (SAM_1k) model to smaller sizes (SAM100m) by extrapolating the set of MBAs found using the SAM orbital element database (all, by definition, with diameters $\geq$1 km) within a specified simulation field. For this extrapolation, we chose the DGJ98 model as parameterized by equation (2) from Tedesco & Désert (2002). In effect, this introduces a slope change at 1 km from the steeper SAM_1k curve to the shallower DGJ98 model slope. Without this slope change, an extrapolation of the SAM_1k model to 100 m results in a population of 44 billion, whereas with it there are 58 million with diameters greater than 100 m. Because of this large difference, we preferred to adopt a more conservative approach, also taking into account that a straightforward extrapolation of SAM_1k to 100 m overlooks the fact that at these sizes a Yarkovsky-driven depletion of the population is likely occurring.

The spatial distribution of the SAM_1k objects is obtained from a two-body ephemeris code, while those for the SAM100m objects are randomly placed in three-dimensional space subject to the constraint that their mean locations and the dispersion of those values match that of the background zone or family class to which they belong.[12] For the remainder of § 5, the term "SAM" refers to the combined SAM_1k model + the SAM100m extrapolation. The above procedure was then used to estimate the numbers, positions, and fluxes of MBAs as small as 100 m lying in a given SAM_1k simulation field.

5.1. *Near-Sun Surveys*

As an example of a relatively large-area, moderate-brightness-limit survey, we use the proposed space-based *Near Earth Space Surveillance* (*NESS*) mission (Hildebrand et al. 2001a, 2001b). Although the *NESS* survey strategy has not yet been decided, for this exercise we assume it will observe the sky within 20° of the ecliptic plane and at solar elongations between 45° and 70° (i.e., between opposition-centered ecliptic longitudes of approximately 110°–135° at the ecliptic). The purpose of this kind of survey is to search for asteroids whose orbits lie partially or wholly within the Earth's orbit. These NEA subgroups are referred to as Atens and inner Earth objects (IEOs) (Michel et al. 2000), respectively. See Tedesco et al. (2000) for a further discussion regarding this kind of survey but at infrared (8 μm) wavelengths.

Because SAM does not yet contain an NEA population model, we cannot use it to investigate the observational characteristics

[12] This method is used to avoid having to create a model containing 58 million sets of orbital elements.

of this population. Thus, we generated the NEA sample brighter than a limiting visual magnitude of 21 using the same model as in the Tedesco et al. (2000) space-based infrared survey simulation. Namely (following Bowell & Muinonen 1994; Muinonen 1998), we considered all Apollo and Aten asteroids, as well as Amor asteroids with perihelion distances less than 1.13 AU, to be Earth-crossing asteroids (ECAs), i.e., asteroids that can currently, or at some time in the future, intersect the capture cross section of the Earth. As before, we treated the IEOs separately from the others. The simulation presented here used the ECA subset of the NEO population, along with the usual assumption that half the NEAs have low (0.05) and half have moderate (0.155) albedos. We then used SAM to simulate the MBAs present in the *NESS* search fields.

Using SAM we find that there are about 12,000 MBAs with diameters greater than 500 m and $V \leq 21$ in a single $\sim$1000 deg^2 *NESS* field. Of these 12,000 MBAs, all but around 1000 have diameters greater than 1 km.

Fortunately, Atens and IEOs have significantly different sky-plane motion vectors than MBAs, with the longitude rates being a better discriminator than the latitude rates. This difference will have to be exploited to identify the NEAs of interest, although, as discussed in the following paragraph, this may not be as trivial to do as it sounds.

Any object with an ecliptic longitude rate greater than $\sim 75'' \text{ hr}^{-1}$ is almost certainly an NEA because only 1.5% of the MBAs in the field move faster than this. However, using the model of Tedesco et al. (2000), during a typical lunation there should be approximately 40 IEOs, 67 Atens, and 438 non-Aten ECAs in a field versus 12,000 MBAs. Therefore, even if only 1.5% of the MBAs have NEA-like motion rates, this amounts to about 200 MBAs. Thus, because about a third of the asteroids in a given field are rapidly moving MBAs, approximately one-third of the fast-moving objects discovered during a given lunation will ultimately turn out to be MBAs, a fact that will only become known after all 638 fast-moving objects have been followed up. Furthermore, Phocaea and Hungaria asteroids, if present in large numbers at small sizes, could further exacerbate the confusion from non-NEA asteroids. It is believed that the parallax afforded by a space-based sensor will help to identify the NEAs, but this has not yet been modeled.

5.2. *Ground-based Opposition Surveys*

As an example of a deep ground-based opposition survey, we chose to model the recently published results from the SDSS (Ivezić et al. 2001) and the recently completed SKADS survey by Davis et al. (2004). The SDSS detected $\sim$13,000 asteroids in 500 deg^2 of sky to an equivalent limiting magnitude at V of 22.2, and the SKADS survey observed approximately 8.6 deg^2 around the opposition point to a limiting V magnitude of about 24. The results for the SDSS are discussed in § 5.3.

Although we modeled both the first and second epoch fields for the SKADS, which were separated by about 10 days, and computed where the SAM_1k objects discovered at the earlier epoch would appear during the second epoch, here we only present results for the first epoch field. SAM predicts that an 8.6 deg^2 SKADS field should contain about 980 MBAs with diameters greater than 1 km and $\sim$6000 with diameters greater than 100 m and $V \leq 24$, respectively.

5.3. *Space-based Infrared Observations and the SDSS*

As examples of small-area, faint limiting brightness infrared observations we use the recently published results from the IDAS by Tedesco & Désert (2002) and the planned (at the time this paper was submitted) *Spitzer* FLS-EPC.[13] IDAS detected 160 ± 32 asteroids deg^{-2} at an 8 μm equivalent flux density limit of $\sim$0.16 mJy. Since this corresponds to a flux density detection limit 2.7 times higher than that of the FLS-EPC, it implies that it will achieve an asteroid diameter detection limit a factor of $\sim$1.6 smaller, i.e., around 0.6 km. Extrapolating SAM from 1.0 to 0.6 km, as described in § 4, gives 2.4 times as many asteroids with $D > 0.6$ km than with $D > 1.0$ km, or, scaling the *ISO* results, 385 ± 80 asteroids deg^{-2} for the sky-plane density in an FLS-EPC 8 μm ecliptic plane map. This compares with the SAM estimate of 430 ± 40 asteroids deg^{-2}.

5.4. *Wavelength- and Sky-Plane-Location-Dependent Effects on Family Observations*

Table 9 presents predictions for family members using the IDAS, FLS-EPC, and SDSS detection limits. The IDAS 12 μm and FLS-EPC 8 μm detection limits were assumed to be 0.60 and 0.06 mJy, respectively, and $V = 22.5$ was taken to be the SDSS limiting detection magnitude (Jurić et al. 2002). The "Big Six" families included in Table 9 are those with more than $\sim$100,000 SAM members with $D > 1$ km (see Table 6).

In Table 9 column (1) is the center of a 1 deg^2 field centered at an ecliptic latitude of 0° or 5° and a solar elongation 115° west of the Sun; column (2) is the survey being modeled to the detection limits described above; column (3) is the total number of SAM asteroids found in the field and the uncertainty from multiple runs on different dates; columns (4) through (9) give for the Adeona, Eos, Eunomia, Massalia, Themis, and Vesta families, respectively, the percent of the asteroids in the field belonging to each of these families; and column (10) gives the percent of asteroids in the field belonging to one of these six families, i.e., the sum of columns (4) through (9).

The results summarized in Table 9 predict the following:

1. To within the precision of the model, the sky-plane density 5° off the ecliptic plane is about 0.6 ± 0.1 that on the ecliptic and, to within the uncertainties, this ratio is independent of the observation wavelength, this value being 0.57, 0.58, and 0.65, with an uncertainty of ± 0.07 for each, for the IDAS, FLS-EPC, and SDSS simulations, respectively.

2. The distribution of asteroids as a function of the SAM population group differs significantly between the 0° and 5° ecliptic latitude fields. About 90% of the asteroids in the 0° field belong to one of the big six families in Table 9, whereas this is true for only about 75% of the asteroids in the 5° field.

3. The proportion of asteroids in the two fields modeled differs for some of the big six families at certain wavelengths. For example, at infrared wavelengths the proportion of Eos members in the 5° field is $\sim$1.5 times that in the 0° field. However, at visual wavelengths this difference is over a factor of 2. The Adeona family members exhibit a similar, but more pronounced, effect, having about 7 times as many members in the 5° infrared fields as in the 0° infrared fields; the difference for the visual fields is over a factor of 8. The Adeona, Eos, Eunomia, and Vesta families all differ in this same sense. However, the Themis and Massalia families differ in the opposite sense. The proportion of Massalia members at both infrared and visual wavelengths is over 9 times greater in the 0° field than in the 5° field.

4. The variation in the proportion of various families between the on-ecliptic and off-ecliptic fields is due to differences in their

[13] A description of the observing rationale and plan for the FLS-EPC can be found at http://ssc.spitzer.caltech.edu/fls/eclip.

TABLE 9

SAM Predictions for the IDAS, FLS-EPC, and SDSS Detection Limits

Ecliptic Latitude (deg) (1)	Survey (2)	No. deg^{-2}[a] (3)	Adeona Family (%) (4)	Eos Family (%) (5)	Eunomia Family (%) (6)	Massalia Family (%) (7)	Themis Family (%) (8)	Vesta Family (%) (9)	Fraction of SAM (%) (10)
0	IDAS	185 ± 15	0.9	1.9	11.8	23.2	36.2	15.3	89.3
0	FLS-EPC	430 ± 40	0.9	1.6	12.6	23.4	35.7	15.7	89.9
0	SDSS	115 ± 10	0.2	1.9	11.4	25.3	19.7	26.9	85.4
±5	IDAS	105 ± 10	6.0	2.6	20.8	2.5	18.2	20.2	70.3
±5	FLS-EPC	250 ± 20	6.3	2.7	24.1	2.4	20.1	22.4	78.0
±5	SDSS	75 ± 5	1.7	4.1	19.4	2.6	10.0	34.4	72.2
Mean Albedo and Sigma			0.07 ± 0.02	0.14 ± 0.04	0.15 ± 0.09	0.21 ± 0.06	0.08 ± 0.03	0.29 ± 0.08	

[a] Rounded to 5.

orbital elements, primarily the inclinations. As shown in Figure 7, this leads to different distributions on the sky.

For example, consider the Eunomia and Themis families, which comprise nearly half of the infrared samples at ecliptic latitudes $\leq 5^\circ$. The mean orbital inclination of their members is about $0\overset{\circ}{.}76$ for the Themis family and $11\overset{\circ}{.}76$ for the Eunomia family. Thus, as shown in Figure 7, the ratio of Themis to Eunomia family members in the ecliptic plane is about 3.8 and decreases to 1.2 near $\pm 5^\circ$ ecliptic latitude and to 0.4 near $\pm 10^\circ$ ecliptic latitude.

For the low-albedo Adeona and Themis families, the FLS-EPC : SDSS proportion ratio is 3.0 ± 1.3, i.e., in the infrared FLS-EPC map there are about 3 times as many MBAs belonging to the Adeona and Themis families as there are in an SDSS image. For the intermediate-albedo Eos and Eunomia families, this ratio is 0.95 ± 0.25, and the ratio for the moderate-albedo Massalia and Vesta families is 0.77 ± 0.18. However, the FLS-EPC : SDSS proportion ratios are not simply a function of albedo but also of the distances and, less importantly, the phase angles of the observed family asteroids.

5.5. *Summary*

Based on the current SAM version and the above exercises, we predict the following:

1. As many as a third of the rapidly moving asteroids in a given near-Sun visual search field to a limiting V magnitude of 21 are MBAs.
2. For near-opposition ecliptic plane surveys to $V \leq 24$, there are about 115 MBAs deg^{-2} with diameters greater than 1 km and $\sim$700 with diameters greater than 100 m.
3. For a 0.06 mJy completeness limit at 8 μm, the *Spitzer* Ecliptic Plane Survey field should contain about 925 ± 185 MBAs, and the field at ecliptic latitude 5° should contain about 400 ± 80 MBAs.[14]
4. The proportions of individual asteroid families among the asteroids in a given field are strongly dependent on ecliptic latitude and substantially different for observations at visual versus infrared wavelengths.

Since work began on creating the SAM, the size of the known asteroid population has increased by an order of magnitude, and the results from deep searches at visible (JM98; Ivezić et al. 2001) and infrared (Tedesco & Désert 2002; Meadows et al. 2004) wavelengths have been published. Thus, SAM version 1 is already outdated. The current version, however, is still a useful tool for simulating the three-dimensional spatial distribution of MBAs at wavelengths between $\sim$0.3 and 70 μm. Furthermore, and more importantly, the current model makes testable predictions that, once observations are obtained, in addition to "testing" the model, will also provide data with which to improve it. The plans for refining SAM are discussed in § 6.

6. FUTURE DEVELOPMENT

Future development will focus on (1) testing and refining the model, (2) extending the model to smaller sizes, (3) adding missing populations, and (4) incorporating other backgrounds. Each of these efforts is described briefly below.

6.1. *Testing and Refining the Model*

As discussed in § 2.2, we plan to improve the model by changing the algorithm for family member generation in order to account for recent results showing the importance of the Yarkovsky effect in determining the inventory and size distribution of family members. A few preliminary tests have already been made, and they suggest that we should not expect major changes in the final asteroid population produced by the model. Apart from technical details of the model, a major impetus for further development of SAM will come from real observations.

Past, current, and future general and specific ecliptic plane "surveys" can be used to refine the model. For example, according to SAM, 54% of all asteroids with diameters greater than 1 km are members of the Eunomia (30%) or Themis (24%) families. However, as illustrated in Table 9, the actual fraction of asteroids in a given field belonging to these two families varies from 11% to 24% for Eunomia, from 10% to 36% for Themis, and from 29% to 49% for the two combined. Thus, observations from which the diameters and family memberships can be deduced will provide the data needed to adjust each of the model's components.

If, as assumed by SAM, the current asteroid population is dominated by family asteroids, then the results from observations can be compared with those generated by SAM and the outcome used to improve the details. That is, the size-frequency and/or albedo distributions can be adjusted on a family-by-family case. This goal requires more than the determination of asteroid sky-plane densities, for although such densities can negate a model that is predicting far too many or too few asteroids above the survey's detection threshold, such observations (e.g., Ivezić et al. 2001 or Tedesco & Désert 2002) do not provide data from which the model's components can be tested. The SDSS and IDAS publications demonstrate this by showing how maps at either visual or infrared wavelengths, respectively, can be used to measure the asteroid sky-plane density but that, unless the asteroids found in the maps can be assigned to specific population groups, they provide little information on the three-dimensional spatial size and albedo distribution of the asteroids observed.

Visible and infrared searches each have their own observational biases. They therefore provide different kinds of information and hence play a complementary role in the search for the asteroid population's size distribution. Thus, in principle, the actual population can be obtained quite directly by observing the same asteroids (with known orbital elements) at both infrared and visual wavelengths. The *Spitzer* Ecliptic Plane Survey will provide some of this information, viz., the infrared part. Visual observations of these *Spitzer* asteroids to obtain orbits, visual fluxes, and colors are planned but by no means certain.

In practice, only fields near solar elongations of 100°–120° can be surveyed near-simultaneously at both visual and mid-infrared wavelengths. This is due to the restriction on space-based infrared sensors to observe within a solar elongation window between about 60° and 120° combined with, for MBA searches, the optimum ground-based search region near the opposition point.

[14] Preliminary results from the FLS-EPC, compared with these predictions, are that: "To sensitivities of 0.1 mJy at 8 μm . . . Our counts are consistent with the extrapolated *ISO* asteroid counts (Tedesco & Désert 2002) and those predicted by the SAM model . . ." and "SAM predicts 0.6 ± 0.1 *(for the ratio of asteroids detected in the $+5^\circ$ field to those in the 0° field)*, in part because of the inclusion of high-inclination, low-albedo asteroid families, which increases the population of asteroids observed at IR wavelengths at higher ecliptic latitudes. The observed FLS-EPC ratio is 0.9. However, significant Poisson errors due to our relatively small sample indicate that this ratio could be as high as 1.4 or as low as 0.5. Because of small number statistics, the FLS-EPC number counts are therefore not conclusive evidence for a different luminosity function with ecliptic latitude, or for a more slowly decreasing population distribution with increased ecliptic latitude, although they are suggestive of this. Further observations are required to obtain a more conclusive picture of asteroid scale height behavior at these wavelengths and flux limits and to determine revised asteroid counts at ecliptic latitudes poleward of $\beta = 5^\circ$." (Meadows et al. 2004, p. 471). The parenthetical phrase in italics was added by the authors of the present paper.

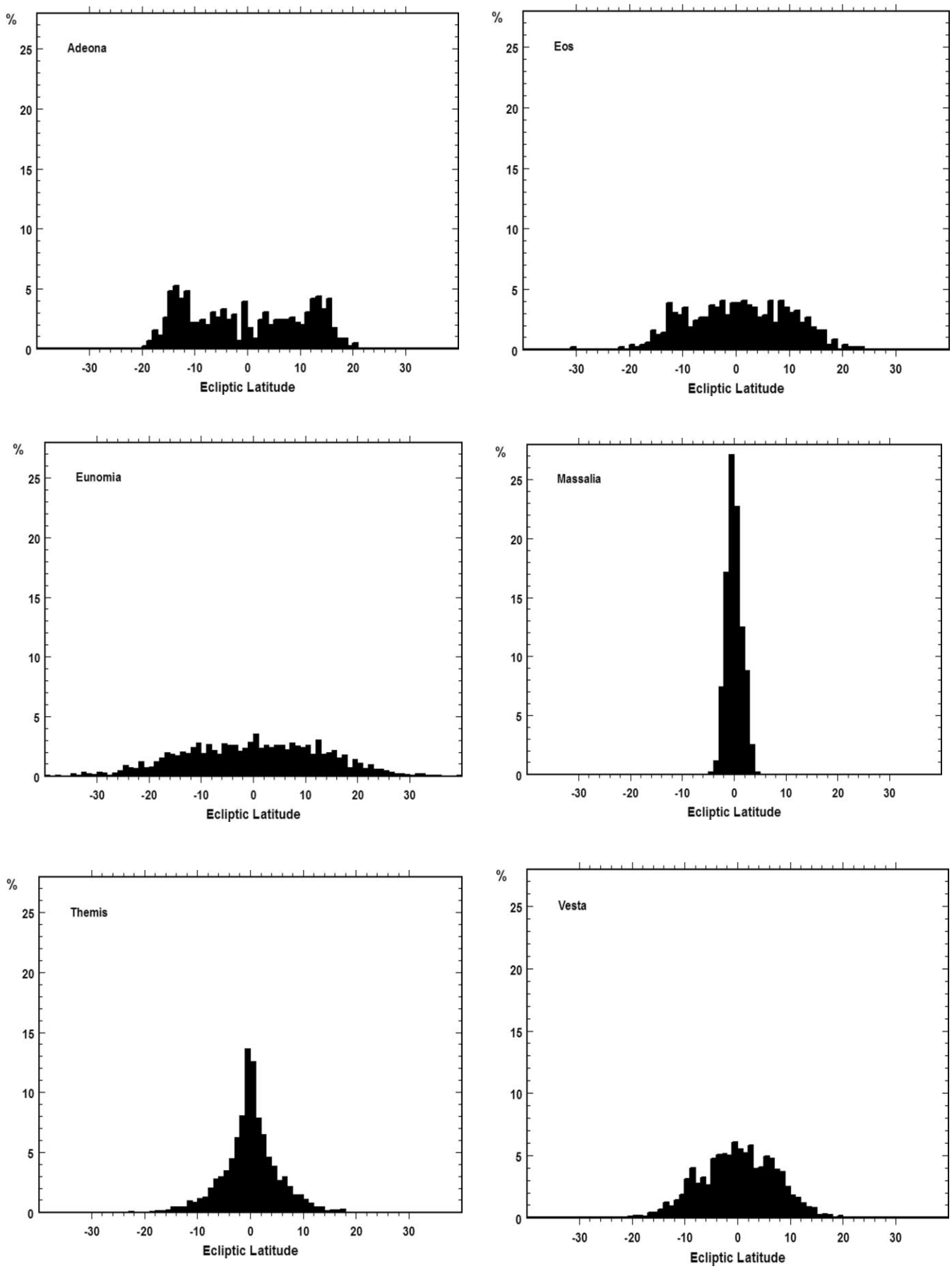

FIG. 7.—Ecliptic latitude distributions for the big six SAM families with solar elongations between 114° and 116° on 2003 March 15.

6.2. *Extending to Smaller Sizes*

As noted in § 4, we have a preliminary model (SAM100m) that will generate asteroids to arbitrarily small sizes, although 100 m is the lower limit for which we have actually run it. SAM100m is useful for estimating the numbers of small, faint asteroids in a field. However, a major shortcoming in using it as an observation planning aid is that it generates *positions*, rather than elements. This is fine if all one wishes to estimate is the number density in a given field as a function of size, albedo, or flux at a given wavelength. But if, as for the Davis et al. (2004) SKADS survey or follow-up for a space-based survey, one wishes to know where these asteroids will be in the future, or where they were in the past, then that cannot be done. At present, only the SAM element file (SAM_1k) presented in § 3 (i.e., the known and statistical asteroid modules) can be used to follow the asteroids in a given scene over time.

In principle, it should not be difficult to generate elements, rather than positions, in SAM100m. These elements will then be written to a file, together with the elements for the SAM_1k asteroids found in the field, and this combined element file is then used to estimate the evolution of these asteroids over time. This is our preferred method for extending the model to smaller sizes because the alternative, expanding the statistical asteroid module from 1 km to 100 m, would increase its size from nearly 2 million records and 170 MB to between 58 million (4.4 GB) and 44 billion records (3.7 TB).

An important caveat is needed when considering sizes smaller than 1 km, because here we enter a domain that is expected to be largely influenced by the Yarkovsky effect (Spitale & Greenberg 2002; Bottke et al. 2002). In this regime, the SFD results from both a continuous replenishment due to the collisional grinding of larger objects and a steady removal due to Yarkovsky drift in the semimajor axis. The resulting slope of the size distribution cannot be easily predicted in this situation and is highly model-dependent. In this sense, great flexibility will certainly be necessary when trying to extend SAM (or any other model) to very small sizes. In this respect, having measured diameters and albedos for a statistically meaningful sample of subkilometer diameter asteroids would certainly prove helpful in developing a realistic model.

6.3. *Adding Missing Populations*

The NEAs (including true NEAs and Mars crossers), the inner main-belt Hungaria and Phocaea and outer main-belt Cybele and Hilda groups, the Jupiter Trojans, and perhaps eventually the Centaur and trans-Neptunian populations as well, will be incorporated into the model.

6.4. *Incorporating Other Backgrounds*

Just as MBAs form the background for faint-limiting-magnitude NEA searches, so too do inertial point sources and the zodiacal cloud, since all share the canvas on which asteroids are observed. Thus, to accurately model a given scene, all of these components must be included.

The importance of each component depends on the geometry and wavelength of observation. For example, for near-Sun observations at visual wavelengths, the zodiacal background is the limiting factor, while for near-opposition searches, it is less important.

7. CLOSING REMARKS

Recent post-SAM estimates of the asteroid belt population with diameters above 1 km are within a factor of 3 of that predicted using SAM. An investigation using *ISO* is in agreement with the SAM model (Tedesco & Désert 2002), while another, using preliminary data from the SDSS (Ivezić et al. 2001), gives results lower by about a factor of 2.6 and with a markedly different SFD as well (see Fig. 4).

At least part of the discrepancy between results from visual surveys and those from infrared surveys is because, for any given distance, visual surveys are biased in favor of discovering larger, higher albedo asteroids and visual data alone cannot be used to accurately derive asteroid diameters. This is because the absolute brightness of an asteroid depends on its cross section and albedo, and asteroid albedos span a range of at least a factor of 12. On the other hand, the infrared flux is only weakly dependent on the albedo. For example, as noted by Tedesco & Désert (2002, p. 2070): "... on 2001 March 26, the 100 km main-belt asteroid 50 Virginia was at a solar elongation of 110°, a typical elongation for space-based infrared observations. Virginia's visual magnitude at this time, given its SIMPS (Tedesco et al. 2002) diameter of 99.82 km, would be 14.5 if its visual geometric albedo were 0.03, and 11.8 if its visual geometric albedo were 0.36, a difference of 2.7 mag. The 12.0 μm magnitudes under these same conditions would be 2.16 and 2.46, respectively, or a difference of only 0.3 mag. Furthermore, the lower albedo would actually result in a slightly higher 12.0 μm brightness because in this case the asteroid's temperature would be higher. Thus, an infrared survey is slightly biased in favor of discovering lower albedo asteroids." Since SAM's SFD is based on diameters, rather than visual magnitudes, and because the diameters are derived primarily from infrared observations, SAM predictions are in better agreement with those from infrared surveys.

While we hope that new observational results (like the SKADS survey mentioned above) will provide new constraints in the near future, we note that SAM provides a number of significant implications for theoretical studies. First, it should ultimately provide the best estimate of the current size distribution down to sizes of 1 km, an input used as an essential constraint in all studies aimed at simulating the collisional evolution of the SFD in the main belt, starting from some primordial population. In addition, the current version of SAM is in reasonable agreement with the size distribution derived by DGJ98 down to sizes around 2 km, where the two distributions diverge, with SAM predicting about twice the number of objects larger than 1 km than the DGJ98 model (see Fig. 6). The general morphology of the SAM and DGJ98 models also differs. In particular, SAM does not confirm the "hump" in the SFD between 3 and 30 km. The existence of this "hump" was interpreted by DGJ98 in terms of collisional physics and size-strength scaling laws. If this hump does not exist, some revision of these models may be necessary. Thus, SAM has important implications for a large number of open theoretical issues, including the general process of collisional evolution of the belt, and the origin of NEAs.

SAM version 1 is an important step toward obtaining the true SFD for MBAs. The comparison with relevant observations and models presented above leads us to believe that the "true" SFD down to diameters of 1 km or below is within reach. We propose to achieve this goal by refining SAM using observations designed expressly for this purpose. Therefore, the next phase is to obtain observations to test *quantitative predictions* made by the current model for specific observational scenarios, some examples of which are presented in § 5, and to use the results of these observations to refine the model.

As we probe the asteroid belt to smaller sizes, new challenges and opportunities will arise. Some of these can be anticipated through simulations such as those made possible by SAM, and

when something unexpected appears, it may be more readily recognized.

The work described herein was made possible through support (to E. T.) from the US Air Force Research Laboratory (contract F19628-98-C-0032), the National Science Foundation (under grant 0073837) and the National Aeronautics and Space Administration under contract S-92517-Z, and grants NNG04GF40G and NNG04GK46G, issued through the Office of Space Science Research and Analysis Programs. It also benefited from discussions with D. Davis, D. Durda, Z. Ivezić, and A. Morbidelli. We wish to thank the referee, Robert Jedicke, for his thorough review.

REFERENCES

Belton, M. J. S., et al. 1992, Science, 257, 1647
Bottke, W. F., Vokrouhlický, D., Rubincam, D. P., & Brož, M. 2002, in Asteroids III, ed. W. Bottke et al. (Tucson: Univ. Arizona Press), 395
Bowell, E., Hapke, B., Domingue, D., Lumme, K., Peltoniemi, J., & Harris, A. W. 1989, in Asteroids II, ed. R. P. Binzel, T. Gehrels, & M. S. Matthews (Tucson: Univ. Arizona Press), 524
Bowell, E., & Muinonen, K., 1994, in Hazards Due to Comets and Asteroids, ed. T. Gehrels (Tucson: Univ. Arizona Press), 149
Bus, S. J. 1999, Ph.D. thesis, MIT
Campo Bagatin, A., Cellino, A., Davis, D. R., Farinella, P., & Paolicchi, P. 1994, Planet. Space Sci., 42, 1079
Cellino, A., Bus, S. J., Doressoundiram, A., & Lazzaro, D. 2002, in Asteroids III, ed. W. Bottke et al. (Tucson: Univ. Arizona Press), 633
Cellino, A., Dell'Oro, A., & Zappalà, V. 2004, Planet. Space Sci., 52, 1075
Cellino, A., Hutton, R. G., Di Martino, M., Bendjoya, P., Belskaya, I. N., & Tedesco, E. F. 2005, Icarus, submitted
Cellino, A., Hutton, R. G., Tedesco, E. F., Di Martino, M., & Brunini, A. 1999a, Icarus, 138, 129
Cellino, A., Michel, P., Tanga, P., Zappalà, V., Paolicchi, P., & Dell'Oro, A. 1999b, Icarus, 141, 79
Cellino, A., Zappalà, V., Doressoundiram, A., Bendjoya, P., Dotto, E., & Migliorini, F. 2001, Icarus, 152, 225
Cellino, A., Zappalà, V., & Farinella, P. 1991, MNRAS, 253, 561
Chauvenet, W. 1863, Theory and Use of Astronomical Instruments, Method of Least Squares, Vol. 2 (4th ed.; Philadelphia: J. B. Lippincott), 558
Davis, D. R., Durda, D. D., Marzari, F., Bagatin, A. C., & Gil-Hutton, R. 2002, in Asteroids III, ed. W. Bottke et al. (Tucson: Univ. Arizona Press), 545
Davis, D. R., Gladman, B., Jedicke, R., & Williams, G. 2004, BAAS, 36, 1142
Davis, D. R., Weidenschilling, S. J., Farinella, P., Paolicchi, P., & Binzel, R. P. 1989, in Asteroids II, ed. R. P. Binzel, T. Gehrels, & M. S. Matthews (Tucson: Univ. Arizona Press), 805
Dell'Oro, A., Paolicchi, P., Cellino, A., Zappalà, V., Tanga, P., & Michel, P. 2001, Icarus, 153, 52
Dunham, D. W. 1992, S&T, 83, 72
Durda, D. D., & Dermott, S. F. 1997, Icarus, 130, 140
Durda, D. D., Greenberg, R., & Jedicke, R. 1998, Icarus, 135, 421 (DGJ98)
Evans, R., et al. 1998, Icarus, 131, 261
Farinella, P., & Davis, D. R. 1994, Lunar Planet. Sci. Conf., 25, 365
Farinella, P., Davis, D. R., Cellino, A., & Zappalà, V. 1992, A&A, 257, 329
Gradie, J. C., Chapman, C. R., & Tedesco, E. F. 1989, in Asteroids II, ed. R. P. Binzel, T. Gehrels, & M. S. Matthews (Tucson: Univ. Arizona Press), 316
Gradie, J., & Tedesco, E. F. 1982, Science, 216, 1405
Gradie, J. C., & Tedesco, E. F. 1988, BAAS, 20, 866
Hanner, M. S., & Cruikshank, D. P. 2000, The Solar System and Circumstellar Dust Disks: Prospects for *SIRTF* (Pasadena: *Spitzer* Science Center), http://ssc.spitzer.caltech.edu/paperstalks/Dana_Point/Hanner.pdf
Hildebrand, A. R., Carroll, K. A., Balam, D. D., Matthews, J. M., Kuschnig, R., Brown, P. G., & Tedesco, E. F. 2001a, in Space Resources Roundtable II (Golden: Colorado School of Mines), 25
Hildebrand, A. R., et al. 2001b, Lunar Planet. Sci. Conf., 32, 1790
Ivezić, Ž., et al. 2001, AJ, 122, 2749
Jedicke, R., Larsen, J., & Spahr, T. 2002, in Asteroids III, ed. W. Bottke, et al. (Tucson: Univ. Arizona Press), 71
Jedicke, R., & Metcalfe, T. S. 1998, Icarus, 131, 245 (JM98)
Jurić, M., et al. 2002, AJ, 124, 1776
Kennealy, J. P., Noah, P. V., Tedesco, E. F., Cutri, R. M., & Dermott, S. F. 1993, Final Report, Apr. 1988–Jan. 1993 (Nashua: Mission Research Corp.)
Kuiper, G. P., Fujita, Y., Gehrels, T., Groeneveld, I., Kent, J., van Biesbroeck, G., & van Houten, C. J. 1958, ApJS, 3, 289
Marzari, F., Davis, D. R., & Vanzani, V. 1995, Icarus, 113, 168
Meadows, V. S., et al. 2004, ApJS, 154, 469
Michel, P. 1999, in The Dynamics of Small Bodies in the Solar System: A Major Key to Solar System Studies, ed. B. A. Steves & A. E. Roy (Dordrecht: Kluwer), 171
Michel, P., Benz, W., Tanga, P., & Richardson, D. C. 2001, Science, 294, 1696
Michel, P., Zappalà, V., Cellino, A., & Tanga, P. 2000, Icarus, 143, 421
Migliorini, F., Michel, P., Morbidelli, A., Nesvorný, D., & Zappalà, V. 1998, Science, 281, 2022
Migliorini, F., Zappalà, V., Vio, R., & Cellino, A. 1995, Icarus, 118, 271
Morbidelli, A., Jedicke, R., Bottke, W. F., Michel, P., & Tedesco, E. F. 2002, Icarus, 158, 329
Morbidelli, A., Nesvorný, D., Bottke, W. F., Michel, P., Vokrouhlický, D., & Tanga, P. 2003, Icarus, 162, 328
Muinonen, K. 1998, Planet. Space Sci., 46, 291
Nesvorný, D., Morbidelli, A., Vokrouhlický, D., Bottke, W. F., & Broz, M. 2002, Icarus, 157, 155
Reach, W. T. 1997, Icarus, 127, 461
Spitale, J., & Greenberg, R. 2002, Icarus, 156, 211
Tanga, P., Cellino, A., Michel, P., & Zappalà, V. 1999, Icarus, 141, 65
Taylor, J. R. 1982, An Introduction to Error Analysis (Mill Valley: University Science Books)
Tedesco, E. F. 1979, Ph.D. thesis, New Mexico State Univ.
———. 1989, in Asteroids II, ed. R. P. Binzel, T. Gehrels, & M. S. Matthews (Tucson: Univ. Arizona Press), 1090
———. 1990, Minor Planet Circ. 17256
———. 1994, in IAU Symp. 160, Asteroids, Comets, Meteorites 1993, ed. A. Milani, M. Di Martino, & A. Cellino (Dordrecht: Kluwer), 55
———. 2000, Research Support for the Analysis and Management of Celestial Backgrounds Data, AFRL-VS-TR-2001–1601
Tedesco, E. F., & Désert, F.-X. 2002, AJ, 123, 2070
Tedesco, E. F., Muinonen, K., & Price, S. D. 2000, Planet. Space Sci., 48, 801
Tedesco, E. F., Noah, P. V., Noah, M., & Price, S. D. 2002, AJ, 123, 1056
Tholen, D. J., & Barucci, M. A. 1989, in Asteroids II, ed. R. P. Binzel, T. Gehrels, & M. S. Matthews (Tucson: Univ. Arizona Press), 298
Van Houten, C. J., Van Houten-Groeneveld, I., Herget, P., & Gehrels, T. 1970, A&AS, 2, 339
Zappalà, V., Bendjoya, P., Cellino, A., Farinella, P., & Froeschlé, C. 1995, Icarus, 116, 291
Zappalà, V., & Cellino, A. 1996, in ASP Conf. Ser. 107, Completing the Inventory of the Solar System, ed. T. W. Rettig & J. M. Hahn (San Francisco: ASP), 29
Zappalà, V., Cellino, A., Gladman, B. J., Manley, S., & Migliorini, F. 1998, Icarus, 134, 176
Zellner, B. 1979, in Asteroids, ed. T. Gehrels (Tucson: Univ. Arizona Press), 783